Title

Toward complete spectroscopy of Lu167

Journal

Physical Review C, 92(6)

ISSN

2469-9985

Authors

Roux, DG

C., W

Hagemann, GB

et al.

Publication Date

2015-12-01

DOI

10.1103/physrevc.92.064313

Peer reviewed

Toward complete spectroscopy of ^{167}Lu

D. G. Roux,[1,*] W. C. Ma,[1] G. B. Hagemann,[2] H. Amro,[1] D. R. Elema,[2] P. Fallon,[3] A. Görgen,[3,†] B. Herskind,[2] H. Hübel,[4] Y. Li,[1] A. O. Macchiavelli,[3] J. C. Marsh,[1] G. Sletten,[2] D. Ward,[3] and J. N. Wilson[2]

[1]*Department of Physics & Astronomy, Mississippi State University, Mississippi State, Mississippi 39762, USA*

[2]*The Niels Bohr Institute, Blegdamsvej 17, DK-2100 Copenhagen, Denmark*

[3]*Lawrence Berkeley National Laboratory, Berkeley, California 94720, USA*

[4]*Helmholtz-Institut für Strahlen- und Kernphysik, University of Bonn, D-53115 Bonn, Germany*

(Received 3 December 2013; revised manuscript received 10 November 2015; published 16 December 2015; publisher error corrected 22 April 2016)

Excited states in ^{167}Lu were populated in the ^{123}Sb(^{48}Ca,4n) reaction at 203 MeV and decay γ rays measured using the Gammasphere spectrometer array. Two triaxial strongly deformed bands were identified previously and interpreted as zero- and one-phonon wobbling excitations. As a result of more extensive band search, the level scheme has been considerably extended to include ten new rotational bands and some 630 γ-ray transitions. A number of interband linking transitions were revealed, so that all but two bands could be connected with each other. Configurations are proposed for all new bands based on measured observables, with the help of cranked shell model calculations. A γ-ray sequence, previously suggested as a triaxial strongly deformed band based on quasiparticle excitations coexisting with the wobbling excitation in the triaxial potential well, has now been determined to be a signature partner of a coupled band, associated with a normal deformed five-quasiparticle configuration. The possibility of two new bands being associated with triaxial deformation is discussed.

DOI: 10.1103/PhysRevC.92.064313 PACS number(s): 21.10.Re, 23.20.Lv, 25.70.Gh, 27.70.+q

I. INTRODUCTION

The study of triaxial strongly deformed (TSD) structures in nuclei around $A = 165$ has attracted considerable interest in the past decade. The wobbling excitation mode, an experimental fingerprint of nuclei with stable triaxial shape, was predicted about 40 years ago [1], and has now been identified in ^{163}Lu [2,3], ^{165}Lu [4], and ^{167}Lu [5], possibly in ^{161}Lu [6], and recently in ^{167}Ta [7]. In addition, TSD structures based on quasiparticle excitations have also been observed in ^{163}Lu [8,9], ^{164}Lu [10], ^{164}Hf [11], ^{168}Hf [12,13], and a few neighboring nuclides. Several theoretical investigations successfully predicted the existence of this island of TSD structures. Among them, systematic cranking calculations employing the ULTIMATE CRANKER (UC) code [14,15] suggest that the TSD minima with deformation parameters $(\varepsilon_2,\gamma) \sim (0.4,\pm 20^\circ)$ in the potential energy surfaces are stabilized by large single-particle shell gaps associated with proton numbers $Z = 71$ and 72 and neutron numbers $N = 94$ and 97 at large triaxiality [16–18]. So far, the $Z = 71$ proton shell gap is clearly well established, where an aligned $i_{13/2}$ quasiproton plays an important role in the development of the stability of these TSD nuclear shapes [19,20]. While a neutron shell gap at $N = 94$ is supported by the observation of wobbling bands in ^{165}Lu, ^{167}Ta, and TSD bands in ^{163}Tm [21,22], the $N = 92$ isotope ^{163}Lu is by far the best example of wobbling excitation where more wobbling bands (higher phonon excitations) are observed and the bands are significantly stronger than those found in other Lu isotopes. A number of linking transitions between the wobbling bands have been identified in ^{163}Lu, including ten of them from TSD2 (1-phonon) to TSD1 (0-phonon), eight from TSD3 (2-phonon) to TSD1, and four from TSD3 to TSD2. Polarization measurements for the $\Delta I = 1$ linking transitions confirmed their predominant $E2$ nature, a characteristic property predicted by theory. This is the only case where the linking transitions between the wobbling bands are strong enough that their electromagnetic character could be firmly established. In addition, a competing TSD band, TSD4, built on quasiparticle excitation, has also been identified. In ^{165}Lu the interband linking transitions from the 2-phonon to the 1-phonon band could not be firmly established.

In ^{167}Lu, only 0-phonon and 1-phonon bands were identified after an exhaustive band search [5]. The weakest band found in the search has an intensity less than 0.3% relative to the yrast band. This paper reports on the full spectroscopy of ^{167}Lu high-spin states found in this data set, with an emphasis on the normal deformed (ND) structures. All previously known bands were extended to higher spins and ten new rotational bands were established. In total some 630 transitions were placed in the level scheme, making it one of the most extensive level schemes in γ-ray spectroscopy. A number of interband linking transitions in the medium- and high-spin regions were identified so that all but two bands could be connected with each other, and the energies of their bandheads have been determined. A γ-ray sequence was previously suggested to be a TSD band based on quasiparticle excitations [23], making ^{167}Lu the second case after ^{163}Lu [9] for the coexistence of TSD bands based on wobbling and quasiparticle excitations in the triaxial potential well. In the current study, however, the sequence has been determined to be a signature partner of a coupled band (Band 4) associated with a ND five-quasiparticle configuration. The possibilities of two new bands being associated with triaxial shapes are discussed.

Section II outlines the experimental details, and is followed by the results in Sec. III. The band crossings and the

*Current address: Department of Physics and Electronics, Rhodes University, 6140 Grahamstown, South Africa.

†Current address: Department of Physics, University of Oslo, N-0316 Oslo, Norway.

configurations of ND bands are analyzed in Sec. IV, and the evidence of possible new TSD bands is discussed in Sec. IV F.

II. EXPERIMENTAL DETAILS AND DATA ANALYSIS

High spin states of the nucleus ^{167}Lu were populated in the ^{123}Sb(^{48}Ca,4n) reaction at a beam energy of 203 MeV, using the 88″ cyclotron at Lawrence Berkeley National Laboratory. The target consisted of a stack of two 520 μg/cm^2 self-supporting foils enriched to 97.7% in ^{123}Sb. At this energy the dominant residuals ^{166}Lu, ^{167}Lu and ^{168}Lu were populated in the approximate ratio 1 : 5 : 2. Coincident γ rays were measured using the Gammasphere spectrometer array (comprising 100 Compton-suppressed Ge detectors in this experiment), and a data set of approximately 2.2×10^9 fivefold, or higher, coincidence events was collected.

In the offline analysis, the data were sorted into a database where the γ-ray energies and detector identification were stored for each event. The RADWARE software package [24] was used to construct three-dimensional (cube) and four-dimensional (hypercube) histograms, and to then analyze the γ-ray coincidence relationships. The RADWARE band search routine was used extensively to look for weak high-spin bands. In addition, an analysis of γ-ray directional correlation from oriented states (DCO ratios) [25] was performed to determine the multipolarity of the γ rays. Gated DCO matrices, with detectors at 32°, 37°, 143°, 148°, and 163° along the x axis, and detectors from 58° through 122° along the y axis, were constructed for each γ-ray sequence. The extracted DCO ratios from coincidence spectra gated by stretched $E2$ transitions fall into two distinct groups centered around 1.0 and 0.6 for stretched quadrupole and dipole transitions, respectively. The DCO ratio values of mixed transitions can be less than 0.6 or larger than 1.0, depending on the mixing ratios. In particular, most mixed $M1/E2$ transitions in the coupled bands have DCO ratios between 0.6 and 1.0. Further discussion of the technique, including the expected DCO ratios of unstretched transitions and different gating conditions, can be found in a previous publication of Ref. [26]. The parity assignments are based on the multipolarities of linking transitions between bands, as well as on coincidence relationships that introduce important constraints in some instances.

III. THE LEVEL SCHEME

Previously, ^{167}Lu was studied at low spin by Barnéoud *et al.* [27], and up to high spins by Yu *et al.*, where five distinct ND structures based on the proton orbitals $[514]\frac{9}{2}^-$, $[541]\frac{1}{2}^-$, $[404]\frac{7}{2}^+$, $[411]\frac{1}{2}^+$, and $[402]\frac{5}{2}^+$ were identified [28]. The new level scheme was too large to fit into a single figure. It is displayed in three separate figures: Fig. 1 for positive-parity structures, Fig. 2 for negative-parity structures, and Fig. 3 showing details of the low-energy part of the level scheme. This was done at the expense of being able to see the interband decays between bands of opposite parity. Such decays have nevertheless been summarized in Figs. 1 and 2. In total, some 630 transitions have been placed in the level scheme. The bands are numbered according to the order of discussion in the text.

The level scheme has now been substantially extended. For example, Bands 8 and 9 were previously observed below spins $\frac{27}{2}$ and $\frac{17}{2}$, but have now been extended to tentative spins of $(\frac{75}{2})$ and $(\frac{89}{2})$, respectively. Many excited multiquasiparticle bands are found to feed the main ND structures. A striking feature of the present level scheme is the amount of interband linking transitions, such as the crosstalk between Bands 8 and 9. A number of them are also identified in the medium- and high-spin regions. As a result, all ND bands have been firmly linked to each other. The band interactions, which are easily recognized by the interband linking transitions, are summarized in Table I to help explain the level scheme construction. Detailed analysis of these interactions are beyond the scope of this paper and will not be discussed. Bands 11 and 12 were reported in our previous publication as TSD bands based on zero- and one-phonon wobbling excitations [5]. Bands 17 and 18 could not be linked to any known structures and, thus, their excitation energies, spins, and parities remain unknown. A γ-ray sequence, previously suggested to be a possible TSD band based on quasiparticle excitations [23], has now been determined to be the $\alpha = -\frac{1}{2}$ signature of Band 4, a coupled ND band. The γ-ray energies, intensities, level energies, spin and parity assignments, as well as DCO ratios for new transitions, are tabulated in the Appendix.

1. Bands 1–4

The bandhead of Band 1, based on the $\pi[404]\frac{7}{2}^+$ Nilsson configuration, was previously established as the ground state of ^{167}Lu [29]. We have now extended the band from $\frac{67}{2}^+$ to $(\frac{97}{2}^+)$, and many new $M1/E2$ transitions connecting the two signatures have been added. The coincidence spectra for the high-spin region, displayed in Fig. 4, clearly show the new transitions near the top of the band (spectra showing the low-spin region were published previously [28]). The band is fed by Bands 2, 3, and 7, and is found to interact with Band 10 via a number of γ -rays between $\frac{61}{2}^+$ and $\frac{49}{2}^+$. One of the linking transitions, the 776-keV line, is visible in Fig. 4(a).

The decay pathways from Band 2 to Bands 1 and 13 have been established. The extracted DCO ratios for the 656-keV ($\frac{23}{2}^- \rightarrow \frac{21}{2}^+$), 565-keV ($\frac{25}{2}^- \rightarrow \frac{23}{2}^+$), and 483-keV ($\frac{27}{2}^- \rightarrow \frac{25}{2}^+$) linking transitions from Band 2 to Band 1 are 0.65(3), 0.68(7), and 0.69(10), respectively. These values are all consistent with stretched dipole ($E1$ or $M1$) character. At higher spins, Band 2 interacts with the negative-parity Band 14 through several crossover $\Delta I = 2$ transitions which are, most likely, stretched $E2$'s. Therefore, a negative parity and corresponding spin values could be determined for Band 2. The parity assignment is further supported by the presence of the $\Delta I = 2$, presumably $E2$, transitions of 657 ($\frac{45}{2} \rightarrow \frac{41}{2}$) and 772 keV ($\frac{41}{2} \rightarrow \frac{37}{2}$) from Band 2 to the negative-parity Band 13. A 781-keV ($\frac{21}{2}^- \rightarrow \frac{19}{2}^-$) linking transition to Band 15 has also been observed. Figure 5 displays spectra representative of Band 2, and the interband linking transitions from Band 2 to Bands 13 and 14 are shown in Fig. 6. It is worth noting that many DCO ratios of $\Delta I = 1$ transitions between the two signatures of Band 2, in the spin regime $\frac{25}{2}^-$ to $\frac{47}{2}^-$, are much larger than the value ∼0.6 expected for stretched

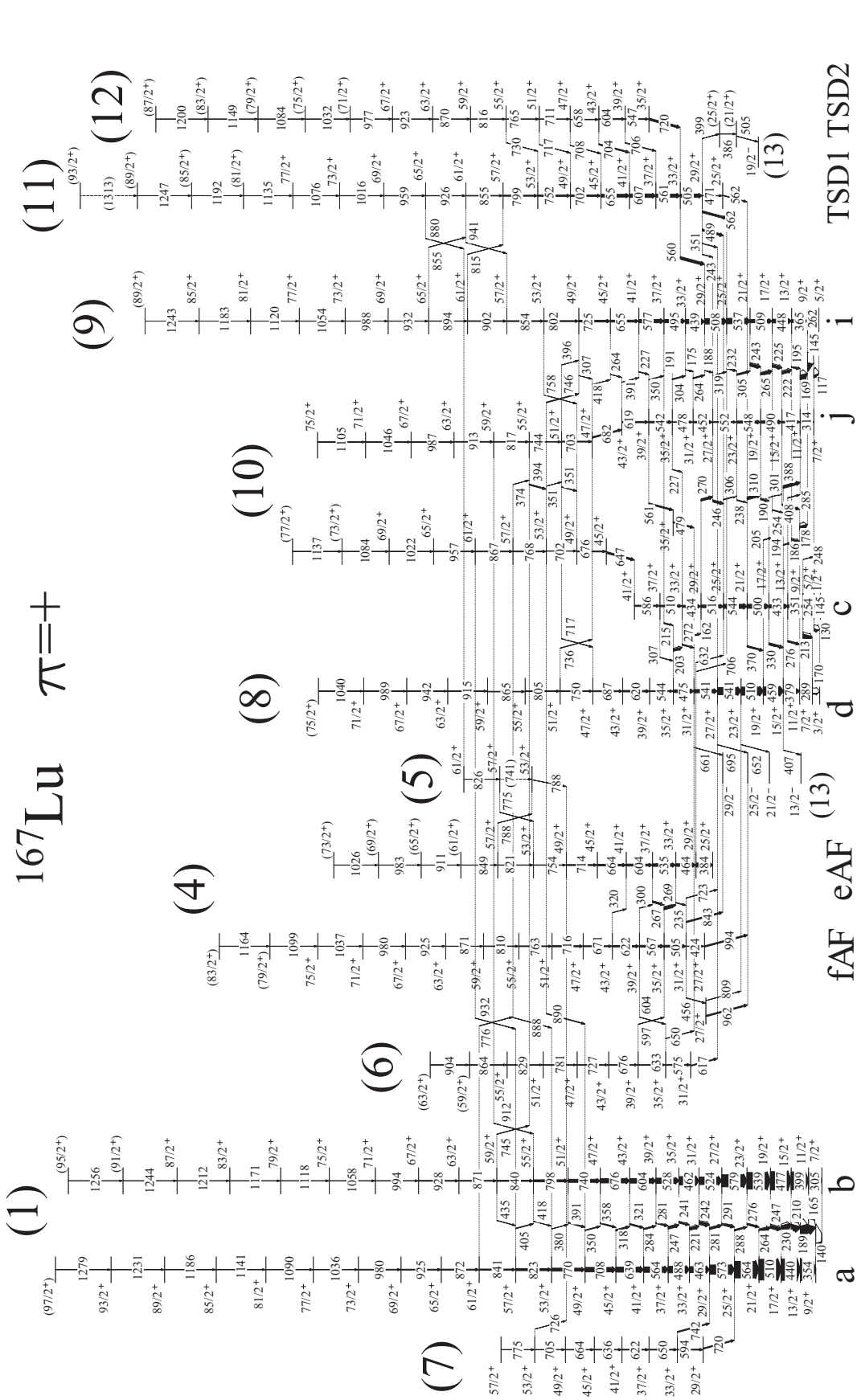

FIG. 1. Positive-parity structures in ^{167}Lu. Gamma-ray energies are in units of keV. Arrow widths indicate transition intensities. Tentative assignments are in parentheses. Decays to negative-parity states in Band 13 are also included in the figure. The labels shown below each γ-ray sequence represent the proposed quasiparticle configurations that will be discussed in Sec. IV.

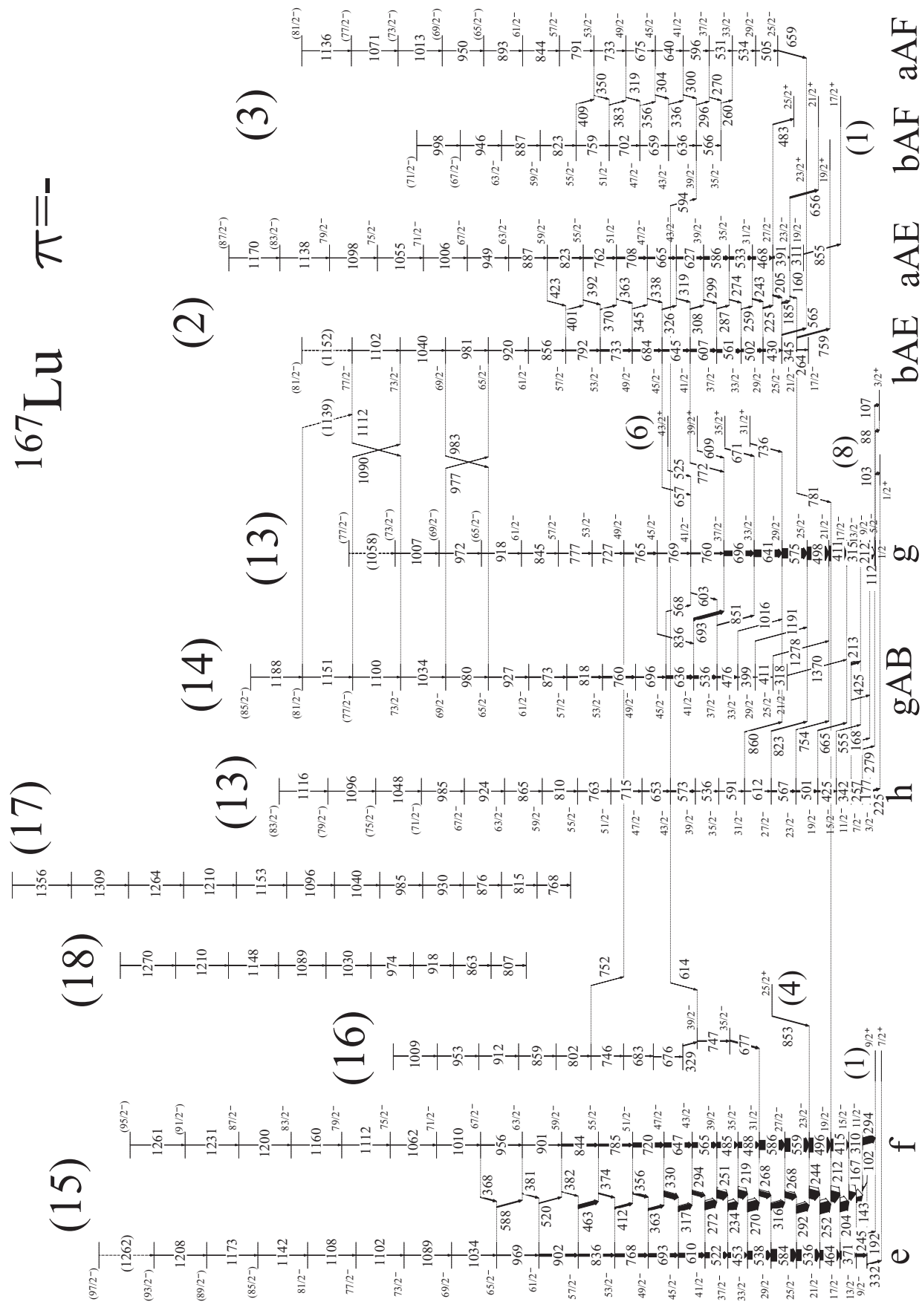

FIG. 2. Negative-parity structures in ^{167}Lu. Transitions between these bands and positive-parity states in Bands 1, 4, 6, and 8 are also shown.

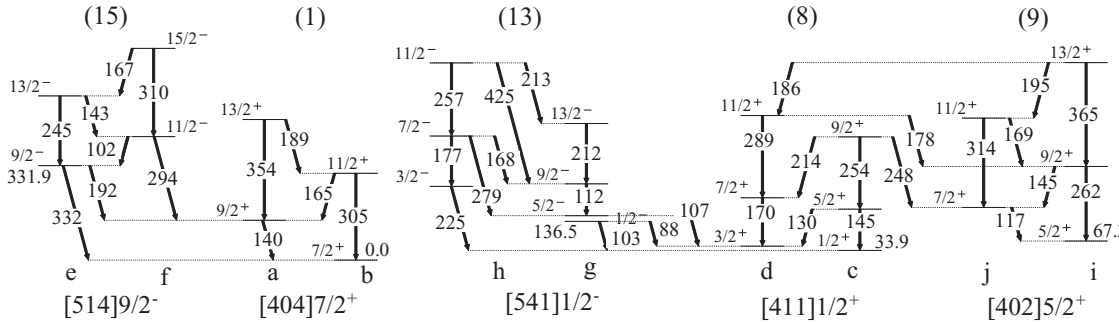

FIG. 3. Low-spin portion of the ^{167}Lu level scheme, showing the bandhead excitation energies. Energies are given in units of keV. Lowercase letters label the participating quasiparticles, and the relevant Nilsson orbitals are given beneath each band. The interband linking transitions at higher spins can be found in Figs. 1 and 2.

$M1$ transitions, suggesting large $E2/M1$ mixing ratios. This will be discussed in Sec. IV A 2.

The decay pathways of Band 3 are fragmented. Only one decay-out transition to Band 1, the 659-keV ($\frac{25}{2}^- \rightarrow \frac{23}{2}^+$) γ ray, could be established. Its DCO value, 0.69(7), is consistent with the stretched dipole interpretation. Since the spins of Band 1 are known from previous work [28], the spins of the levels in Band 3 could be suggested. Further, Band 13 (labeled h) feeds the band via the 594-keV ($\frac{43}{2}^- \rightarrow \frac{39}{2}^-$, $\Delta I = 2$) transition, visible in the spectrum in Fig. 7(c). The most plausible interpretation for this decay is stretched $E2$, suggesting that Bands 3 and 13 have the same (negative) parity. Representative coincidence spectra for Band 3 are shown in Fig. 7.

One of the signature partners of Band 4, the negative signature (labeled as fAF), was reported in reference [23] as a decoupled band. It was suggested there that the band may be a candidate TSD band with negative parity, based on the measured mixing ratio for a single γ ray, the 962-keV decay to the $\frac{25}{2}^-$ state of Band 13. The mixing ratio ($\Delta = -0.5^{+0.50}_{-0.82}$) established in that work indicated mixed $M1/E2$, $\Delta I = 1$ character for the 962-keV transition, even though the value $\Delta = 0$ (i.e., pure stretched dipole) cannot be ruled out on account of the large errors. In this work, however, an important extension of the level scheme is the identification of the signature partner of the fAF sequence, a new sequence of stretched $E2$ transitions labeled as eAF. The two sequences are indeed connected by several linking transitions and their rotational properties, to be discussed in Sec. IV A 4 in detail,

TABLE I. Summary of band interactions. Spin and energy separation for each pair of interacting bands at their closest approach.

Band no.	Band no.	Spin ($\hbar$)	ΔE (keV)
1	10	$\frac{57}{2}^+$	65.8
2	13	$\frac{41}{2}^-$	12.4
2	14	$\frac{65}{2}^-$	1.3
3	13	$\frac{39}{2}^-$	21.5
4	5	$\frac{53}{2}^+$	33.9
4	6	$\frac{39}{2}^+$	29.6
4	7	$\frac{49}{2}^+$	21.0
5	11	$\frac{61}{2}^+$	45.9
8	9	$\frac{31}{2}^+$	20.0
8	10	$\frac{47}{2}^+$	14.2
9	10	$\frac{49}{2}^+$	45.2
9	11	$\frac{61}{2}^+$	39.3

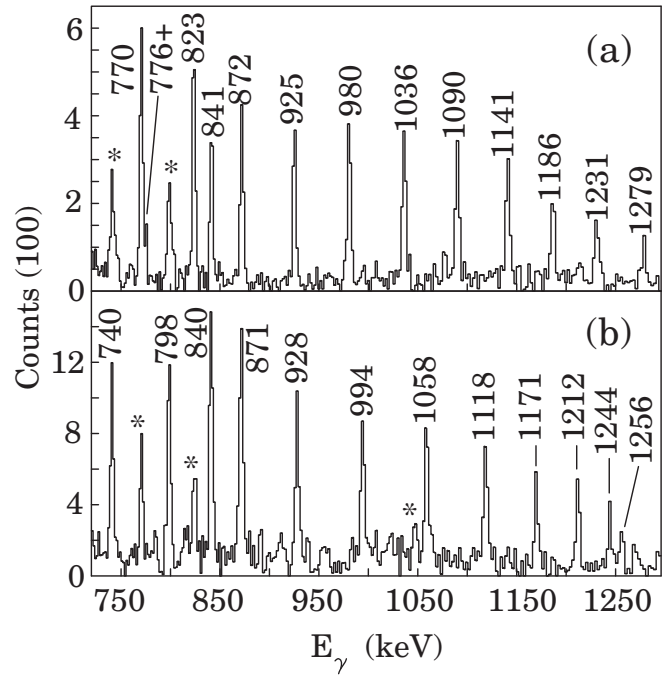

FIG. 4. Fourfold coincidence spectra for the high spin region of Band 1. (a) Positive signature, from a sum of coincidences between transitions above $\frac{57}{2}^+$. (b) Negative signature, showing summed coincidences between two γ rays in gate list a and one in b, where a includes the transitions between the $\frac{95}{2}^+$ and $\frac{63}{2}^+$ levels, and b those between $\frac{49}{2}^+$ and $\frac{9}{2}^+$ in the positive and also $\frac{55}{2}^+$ and $\frac{7}{2}^+$ in the negative signature. The in-band transitions are labeled by energies. The following sign convention is used for the spectra in all figures: the stars ($*$) denote coincidence γ rays in other known bands, the plus signs ($+$) indicate interband linking transitions, the tilde signs ($\sim$) mark the γ rays on the decay-path directly *above* the links, and the pound symbols (#) those below the links.

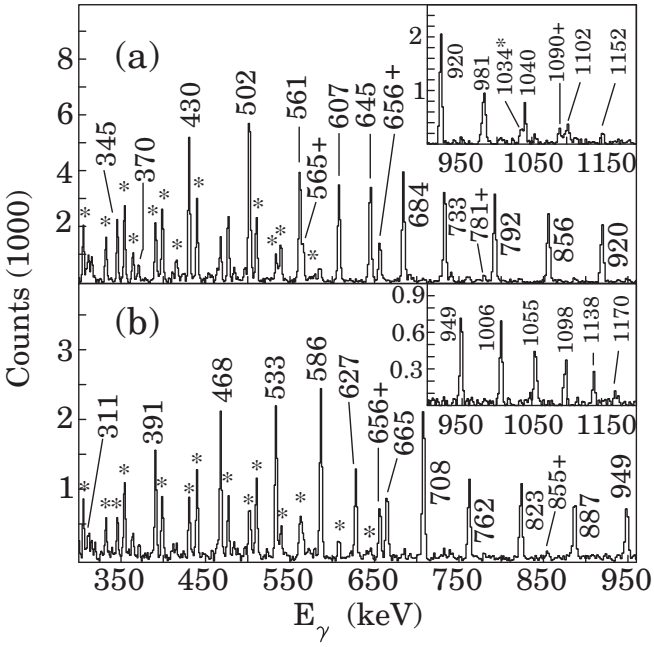

FIG. 5. Fourfold coincidence spectra of Band 2, (a) positive signature, from a sum of triple gates on transitions between $\frac{33}{2}^-$ and $\frac{73}{2}^-$, and (b) negative signature, from a sum of triple gates on transitions between $\frac{39}{2}^-$ and $\frac{79}{2}^-$. The symbols are defined in the caption of Fig. 4.

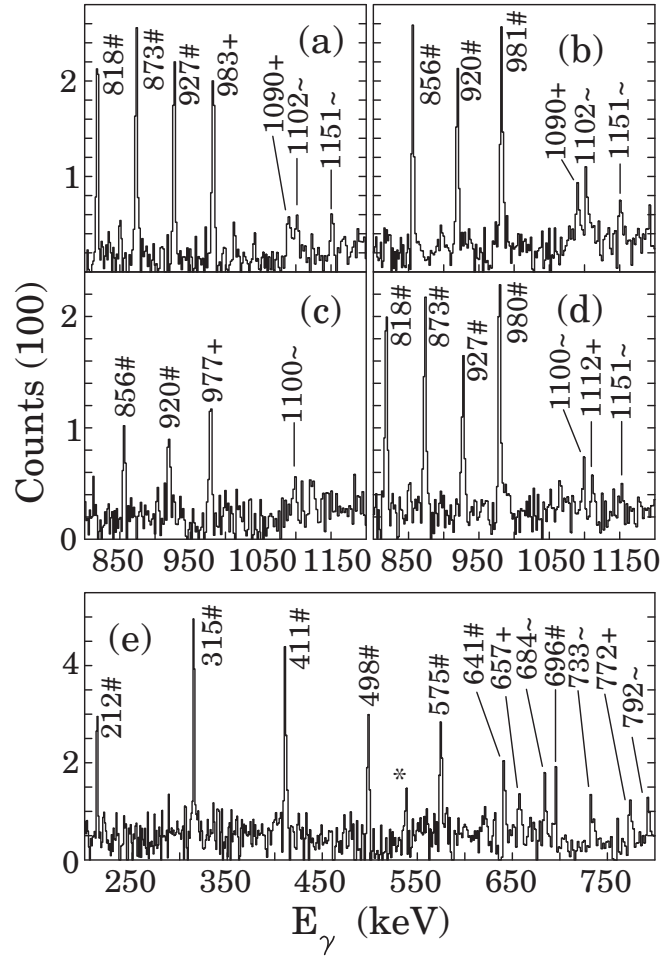

FIG. 6. Fourfold coincidence spectra showing important linking transitions between Bands 2 and 14, and Bands 2 and 13. The spectra are based on the following gate lists: List *a* comprised seven members of Band 14, and list *b* eight members of Band 2, directly below $\frac{65}{2}^-$ in the respective bands. List *c* contained four members of Band 13 directly below $\frac{41}{2}^-$, and list *d* six members of Band 2 directly above $\frac{45}{2}^-$. (a) Coincidence spectrum between 1040 keV and list *a*, showing the 1090- and 983-keV decays between Bands 2 and 14. (b) Coincidences between 1040 keV and *b*, showing the 1090-keV decay from Band 14 to 2. (c) Coincidences between 1034 keV and *b*, showing the 977-keV decay from Band 14 to 2. (d) Coincidences between 1034 keV and *a*, showing the 1112-keV decay from Band 2 to 14. (e) Coincidences between two γ rays in *c* and one in *d*, showing the 657- and 772-keV decays from Band 2 to 13. The symbols are defined in the caption of Fig. 4.

indicate that they form a coupled band. Coincidence spectra for Band 4 are shown in Fig. 8. In this work the band has been connected to Bands 5, 6, 7, 8, 9, 13, and 15 via thirteen interband linking transitions, which can be found in Table IV. While most of these transitions are visible in Fig. 8, some of them can be seen better in other spectra under different coincidence gating conditions. As an example, the 632- ($\frac{29}{2}^+ \rightarrow \frac{25}{2}^+$) and 706-keV ($\frac{29}{2}^+ \rightarrow \frac{25}{2}^+$) transitions from Band 4 to Bands 8 and 9 are presented in Fig. 9, together with the 880–826–775-keV decay pathway from Band 11 to Band 4. The 604-keV ($\frac{39}{2}^+ \rightarrow \frac{35}{2}^+$) decay to Band 6 becomes obvious in a fourfold coincidence spectrum triple-gated on the 622- or 575-keV transition and high-spin members in Band 4.

The DCO ratios of the 962- ($\frac{27}{2}^+ \rightarrow \frac{25}{2}^-$) and 843-keV ($\frac{31}{2}^+ \rightarrow \frac{29}{2}^-$) decay γ rays to Band 13 were extracted to be 0.53(11) and 0.50(10), respectively, and that for the 853-keV ($\frac{25}{2}^+ \rightarrow \frac{23}{2}^-$) transition to Band 15 was found to be 0.63(13). All these values are close to 0.6, a value expected for stretched dipole transitions. Therefore the spins established in the present level scheme are the same as those in Ref. [23]. Furthermore, it is likely that these γ rays have stretched $E1$ character, as $M1$ transitions usually mix with $E2$ and result in different DCO ratios. Since Bands 13 and 15 have negative parity [28], Band 4 probably has a positive parity. Such a scenario is strongly supported by the fact that the band is linked to several positive-parity bands by $\Delta I = 2$ transitions, viz., 723-keV ($\frac{31}{2}^+ \rightarrow \frac{27}{2}^+$), 632-keV ($\frac{29}{2}^+ \rightarrow \frac{25}{2}^+$), and 809-keV ($\frac{27}{2}^+ \rightarrow \frac{23}{2}^+$) decays to Band 8, the 706-keV ($\frac{29}{2}^+ \rightarrow \frac{25}{2}^+$) transition to Band 9, and the 726-keV ($\frac{53}{2}^+ \rightarrow \frac{49}{2}^+$) γ-ray from Band 7 to Band 4. All these linking transitions are likely stretched $E2$'s. If the band were instead assigned negative parity, then such $\Delta I = 2$ linking transitions would have to be $M2$ or $E3$, a much less likely scenario. Furthermore, a mixing is observed between Band 4 and the positive-parity Band 6 through the crossover 604- and 597-keV transitions, which indicates that the two bands should have the same parity. All these facts overwhelmingly lead to a positive parity for Band 4, rather than the previously suggested negative parity [23].

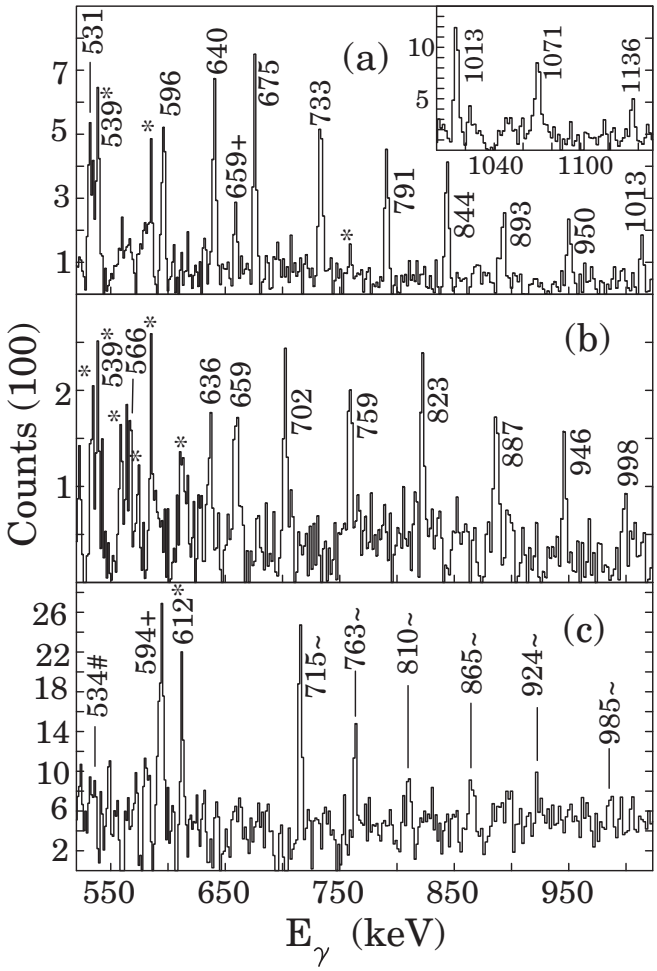

FIG. 7. Spectra for Band 3. Panel (a) shows the positive signature, obtained by summing fourfold coincidences between in-band transitions in the spin range $\frac{25}{2}^-$ to $\frac{65}{2}^-$. The spectrum in the inset emphasizes the high-spin region, and was constructed by summing double-gated spectra from the upper part of the band. The 659-keV linking transition to Band 1 is clearly visible, as is the strong 539-keV transition in that band. Note that the spectrum is free from any transitions in the negative signature. Therefore, the 659-keV is, indeed, a decay-out rather than that in the negative signature. Panel (b) shows the negative signature, obtained by summing fourfold coincidences between in-band transitions in the spin range $\frac{35}{2}^-$ to $\frac{71}{2}^-$. The peak at 659 keV is largely due to the in-band transition, rather than the link to Band 1. Panel (c), which emphasizes the important 594-keV linking transition from Band 13 to Band 3, was generated by summing three-fold coincidences between 653 keV (immediately *above* the link) and 566 and 296 keV (immediately *below* the link). The symbols are defined in the caption of Fig. 4.

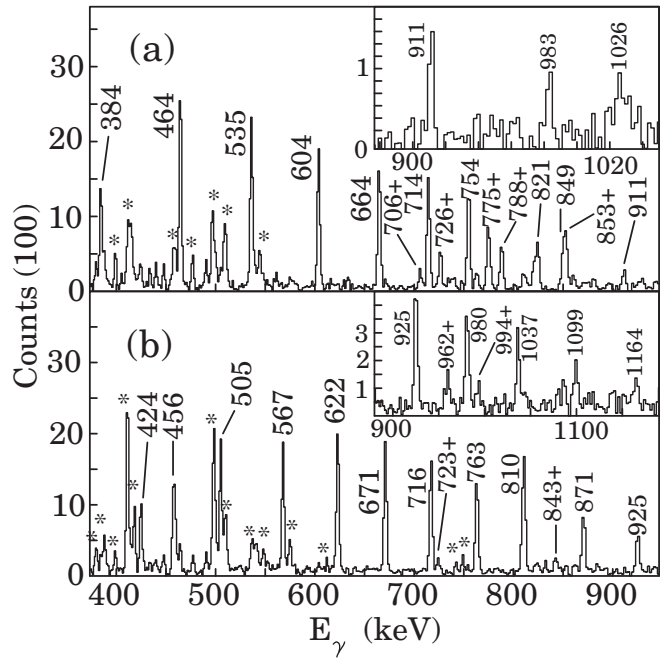

FIG. 8. Coincidence spectra for Band 4. Insets show the topmost transitions. (a) Spectrum for the positive signature. The main panel shows the sum of fourfold coincidence spectra obtained by gating on the six in-band transitions immediately above $\frac{25}{2}^+$. The inset shows summed fourfold coincidence spectra obtained by gating on the last-mentioned sequence and also the transitions above $\frac{49}{2}^+$. (b) Spectrum for the negative signature, obtained by gating on the seven in-band transitions immediately above $\frac{27}{2}^+$. The inset shows summed fourfold coincidence spectra obtained by gating on the last-mentioned sequence and also the six in-band transitions above $\frac{55}{2}^+$. The symbols are defined in the caption of Fig. 4.

The spins and the parity of this band could thus be firmly established.

2. Bands 5–7

Band 5 is a short but very important decay sequence, providing the hitherto "missing link" between TSD and ND structures. It is connected to Band 4 by decay-out transitions of 775- ($\frac{57}{2}^+ \rightarrow \frac{53}{2}^+$) and 788-keV ($\frac{53}{2}^+ \rightarrow \frac{49}{2}^+$), and via another 788-keV ($\frac{57}{2}^+ \rightarrow \frac{53}{2}^+$) transition which feeds the band from Band 4. The measured DCO ratio of 0.99(20) for the 775-keV γ ray indicates its stretched $E2$ character and, thus, a positive parity for the band. The spin and parity assignments are strongly supported by the presence of mixing between Bands 4 and 5 through the 775- and 788-keV crossover transitions at $\frac{57}{2}^+$ level. It is also consistent with the observed 880–826–775-keV decay pathway from Band 11 to Band 4. The 880- and 826-keV γ rays change spins by $4\hbar$. Most likely, both of them are stretched $E2$'s, rather than two $M2$'s or a dipole plus an octupole transition.

Band 6 is connected to Bands 4, 8, and 13, and several interband linking transitions may be seen in the coincidence spectrum in Fig. 10(a). The DCO ratios of the 736- ($\frac{31}{2}^+ \rightarrow \frac{29}{2}^-$), 671- ($\frac{35}{2}^+ \rightarrow \frac{33}{2}^-$), 609- ($\frac{39}{2}^+ \rightarrow \frac{37}{2}^-$), and 525-keV ($\frac{43}{2}^+ \rightarrow \frac{41}{2}^-$) linking transitions to Band 13 are 0.67(13), 0.64(6), 0.64(3), and 0.69(3), respectively. These values are consistent with stretched dipole character. Therefore, the spins may be suggested for the band. Furthermore, the band decays to Band 8 via 617-keV ($\frac{31}{2}^+ \rightarrow \frac{27}{2}^+$) and 650-keV ($\frac{35}{2}^+ \rightarrow \frac{31}{2}^+$) transitions. These $\Delta I = 2$ γ rays are, most likely, stretched $E2$'s, indicating that the band has a positive

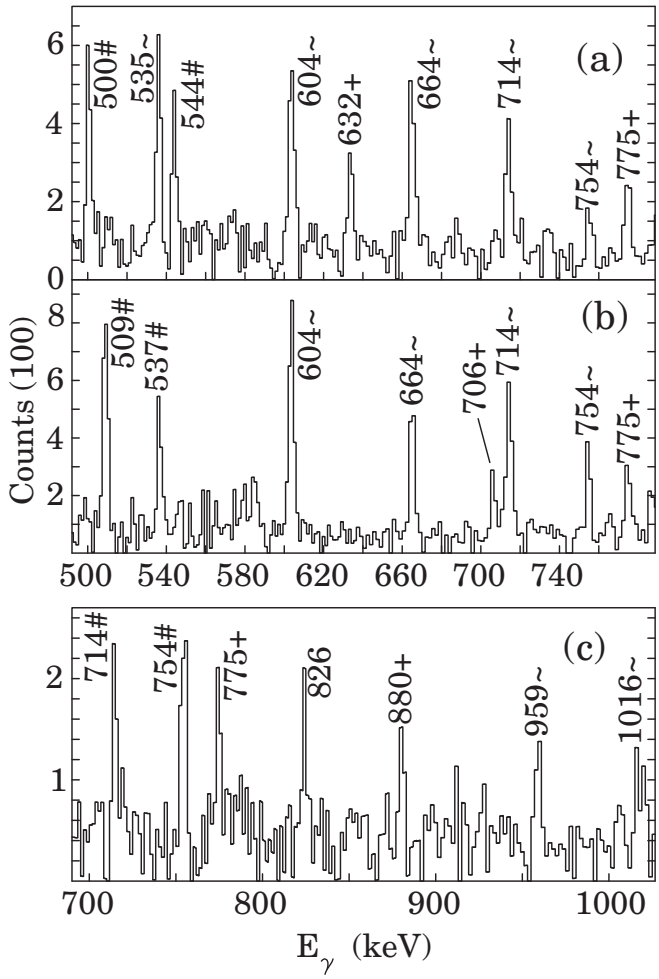

FIG. 9. Coincidence spectra showing crucial interband transitions connecting Band 4 to Bands 5, 8, and 9 in panels (a) and (b), and those connecting Bands 11 and 4 in (c). Each spectrum shows summed fourfold coincidences between gate lists immediately above and immediately below the respective linking transitions. Panel (a) shows the 632-keV decay from the $\frac{29}{2}^+$ state in Band 4 to the $\frac{25}{2}^+$ state in Band 8, (b) shows the 706-keV decay from the $\frac{29}{2}^+$ state in Band 4 to the $\frac{25}{2}^+$ state in Band 9, while (c) shows the 880-, 826-, 775-keV decay pathway from Band 11 to 4. The 775-keV decay from the $\frac{57}{2}^+$ state in Band 5 to Band 4 is visible in all three spectra. The symbols are defined in the caption of Fig. 4.

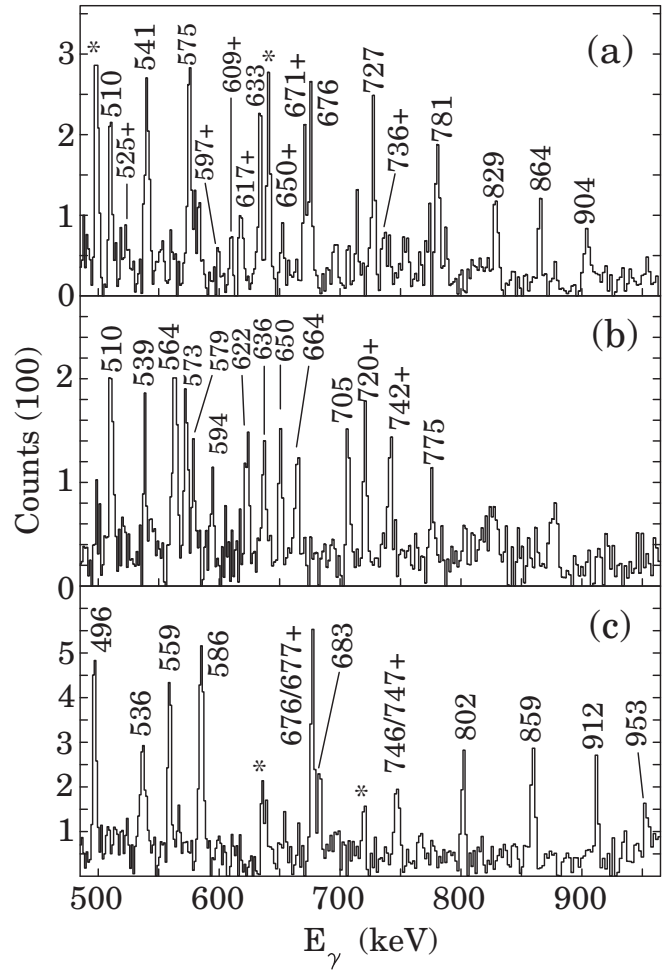

FIG. 10. Summed fourfold coincidence spectra for Bands 6, 7, and 16. Panel (a) shows the sum of triple gates set on transitions between $\frac{31}{2}^+$ and $\frac{59}{2}^+$ in Band 6, while in (b) the gates were set on transitions between $\frac{29}{2}^+$ and $\frac{57}{2}^+$ in Band 7, and in (c) on transitions between $\frac{31}{2}^-$ and $(\frac{69}{2}^-)$ in Band 16. Some of the strong peaks at the extreme left have been truncated. The symbols are defined in the caption of Fig. 4.

parity. The positive parity assignment of the band is consistent with that of Band 4. The interaction between Bands 4 and 6 at $\frac{39}{2}^+$ level, through the crosstalk 597- and 604-keV transitions, indicates that the two bands have the same parity.

Band 7 decays to Band 1 via two transitions, namely 720 keV ($\frac{29}{2}^+ \rightarrow \frac{25}{2}^+$) and 742 keV ($\frac{33}{2}^+ \rightarrow \frac{29}{2}^+$), which can be seen in the coincidence spectrum for the band, in Fig. 10(b). The respective DCO ratios [0.94(9) and 0.96(5)] are consistent with stretched $E2$ character. Thus the spins and positive parity could be determined. The band interacts with Band 4 via a $\Delta I = 2$, presumably $E2$, 726-keV transition which links the $\frac{53}{2}^+$ level with $\frac{49}{2}^+$ in Band 4. This 726-keV linking transition is clearly visible in Fig. 8(a).

3. Band 8–10

A series of six transitions below $I^\pi = \frac{27}{2}^+$, previously associated with the negative signature (d) of the $\pi[411]\frac{1}{2}^+$ orbital [28], and labeled Band 8 in this work, has now been extended to $(\frac{75}{2}^+)$. A coincidence spectrum showing this γ-ray sequence is displayed in Fig. 11(a). In addition, we observe the positive signature partner (c) for the first time. The upper part of this signature continues above $\frac{41}{2}^+$ as Band 10. Four $E1$ transitions are found to decay from the states between $\frac{15}{2}^+$ and $\frac{31}{2}^+$ in signature d of Band 8 and feed Band 13, the $\pi[541]\frac{1}{2}^-$ band.

The lower portion of Band 9 was previously observed below $\frac{17}{2}^+$, and was associated with the $\pi[402]\frac{5}{2}^+$ orbital [28]. The signature i of Band 9 is now observed up to $(\frac{89}{2}^+)$. A coincidence spectrum showing this γ-ray sequence is

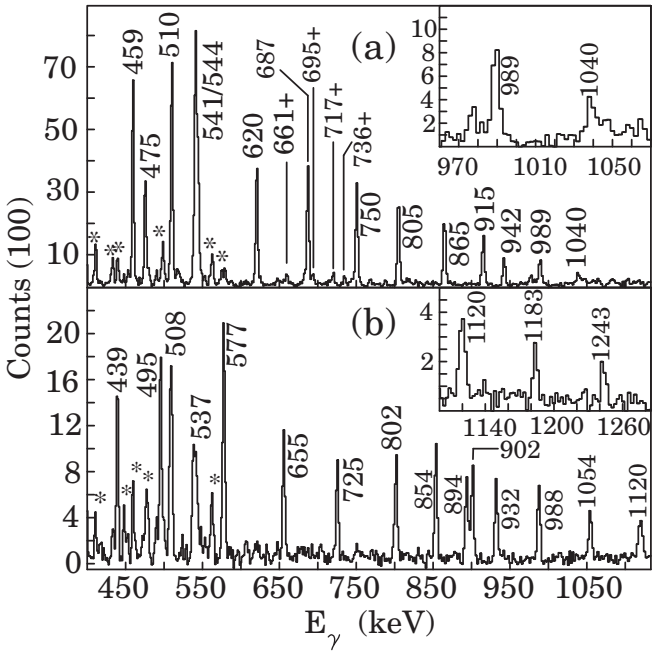

FIG. 11. Summed fourfold coincidence spectra for Bands 8 and 9. In panel (a) triple gates were set on transitions above the $\frac{23}{2}^+$ level of Band 8, and in (b) on transitions above the $\frac{41}{2}^+$ level of Band 9. The symbols are defined in the caption of Fig. 4.

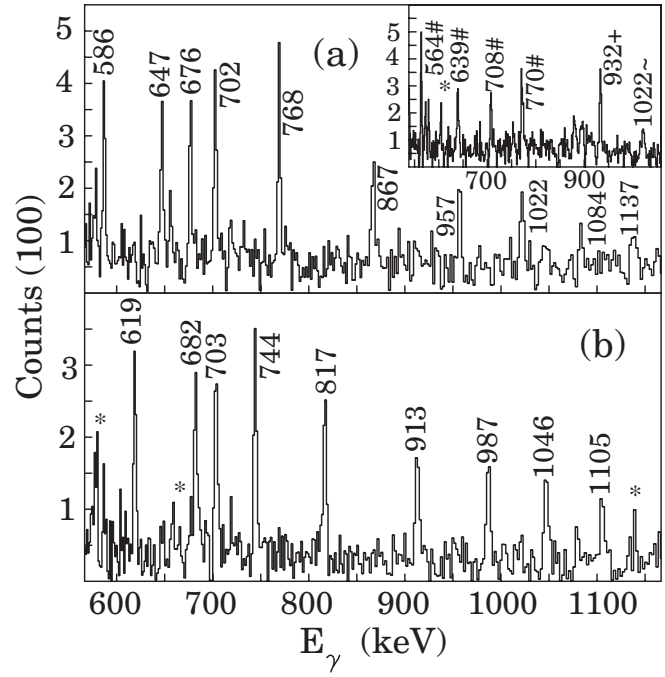

FIG. 12. (a) Summed fourfold coincidence spectrum for the positive signature of Band 10, from a sum of triple gates on transitions between $\frac{37}{2}^+$ and $(\frac{73}{2}^+)$. The inset shows a threefold coincidence spectrum with gates set on the 957-keV transition populating $\frac{61}{2}^+$ in Band 10 and the 823-keV transition depopulating $\frac{57}{2}^+$ in Band 1. The 932-keV $\frac{61}{2}^+ \rightarrow \frac{57}{2}^+$ interband decay is clear. (b) Fourfold coincidence spectrum for the negative signature of Band 10, from a sum of triple gates on transitions between $\frac{39}{2}^+$ and $\frac{71}{2}^+$. The symbols are defined in the caption of Fig. 4.

displayed in Fig. 11(b). The upper part of the signature j continues above $\frac{43}{2}^+$ as Band 10, and extends up to $\frac{75}{2}^+$. At low spins Bands 8 and 9 become nearly degenerate, and extensive crosstalk between the two indicates substantial mixing. Significant structures decaying to Band 9 include Bands 10, 11, and, indirectly, 12.

Band 10 is interesting in that it feeds into all of the main positive-parity sequences and, as discussed in Sec. IV, undergoes structural metamorphosis with increasing spin. The bulk of the intensity from this band feeds into the lower part of Bands 8 and 9, but it is also seen to interact with the Band 1. The spectra for Band 10 are displayed in Fig. 12.

The excitation energy of the bandhead for Band 8 (at $I^\pi = \frac{1}{2}^+$) was not known before, and is now established as 33.9 keV (see Fig. 3), on the basis of several stretched $E2$ linking transitions between Band 10 and the ground-state band, Band 1. The relevant transitions are 890 ($\frac{53}{2}^+ \rightarrow \frac{49}{2}^+$), 888 ($\frac{57}{2}^+ \rightarrow \frac{53}{2}^+$), 912 ($\frac{59}{2}^+ \rightarrow \frac{55}{2}^+$), and 932 keV ($\frac{61}{2}^+ \rightarrow \frac{57}{2}^+$) from Band 10 to Band 1, and the 776- ($\frac{61}{2}^+ \rightarrow \frac{57}{2}^+$) and 745-keV ($\frac{59}{2}^+ \rightarrow \frac{55}{2}^+$) γ rays from Band 1 to Band 10. The DCO ratio of 0.93(14) for the 932-keV γ ray is consistent with stretched $E2$ character. This further confirms the spins and positive parity of Band 10. Our placement of the $\frac{3}{2}^+$ level in Band 8 differs from the initial work of Barnéoud and Foin [27]. This point is taken up again in the discussion on Band 13 (Sec. III 5).

4. Bands 11 and 12

Bands 11 and 12 were reported in our previous work [5], where they were called TSD1 and TSD2. Band 11 is directly connected to Bands 8 and 9. At low spins it decays to Band 9 via three transitions (562, 243, and 560 keV), and to Band 8 via another three transitions (562, 489, and 351 keV). At higher spins it interacts once again with Band 9 via a further three transitions (941, 855, and 815 keV), and the band is linked via the 880-keV transition to the $\frac{61}{2}^+$ state in Band 5. This important decay pathway links the TSD band to the remaining major ND structures: Band 5 decays to Band 4, which in turn decays to Bands 8, 13, and 15. The mixing of ND and TSD structures, indicated by the cross talk between TSD1 (Band 11) and Bands 9 and 5, has been discussed in Ref. [23]. We note here that Band 12 (TSD2) decays to Band 11 (TSD1) via six $\Delta I = 1$ mixed $M1/E2$ transitions of predominantly $E2$ character. This is the characteristic signature of wobbling excitations [5].

5. Bands 13 and 14

The positive signature g in Band 13 and Band 14, previously observed up to $\frac{49}{2}^-$ and $\frac{65}{2}^-$ [28], have now been extended to $(\frac{77}{2}^-)$ and $(\frac{85}{2}^-)$, respectively. The negative signature h of Band 13, previously seen up to $\frac{19}{2}^-$ [27], has now been substantially extended to a tentative $(\frac{83}{2}^-)$ state. Coincidence spectra for Bands 13 and 14 are shown in Fig. 13. The signature h decays to the signature g via several $\Delta I = 1$ transitions.

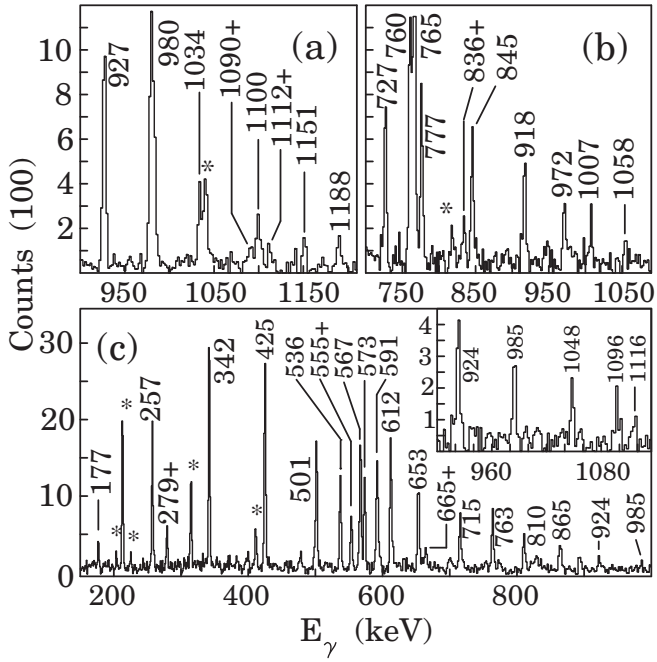

FIG. 13. Summed fourfold coincidence spectra for Bands 13 and 14. (a) The high-spin region of Band 14, based on gates set on in-band transitions between $\frac{25}{2}^-$ and $(\frac{77}{2}^-)$. A spectrum showing the low-spin portion was previously reported in Ref. [28]. (b) The high-spin part of the positive signature of Band 13. Gates were set on in-band transitions between $\frac{9}{2}^-$ and $(\frac{73}{2}^-)$. The peaks at 760 and 765 keV have been truncated. (c) Spectra showing the negative signature of Band 13, based on gates set on γ-rays between $\frac{15}{2}^-$ and $(\frac{79}{2}^-)$. The inset emphasizes the high spin part of the band. Note that γ rays not included in the gate list may show enhanced intensities. The symbols are defined in the caption of Fig. 4.

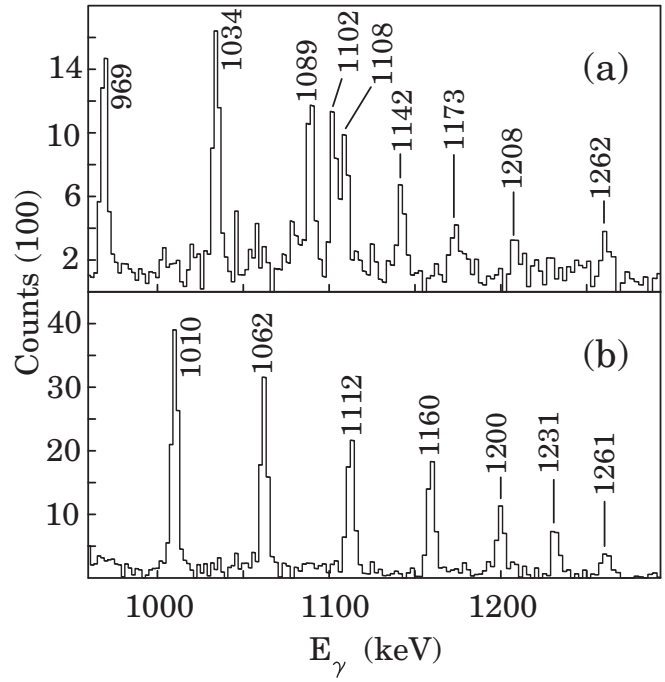

FIG. 14. Summed fourfold coincidence spectra showing the high-spin region of Band 15. The spectra are based on the following gate lists: list *a* comprised nine members above $\frac{53}{2}^-$ in the positive-signature sequence, list *b* ten members above $\frac{51}{2}^-$ in the negative-signature sequence, and list *c* contained most transitions below $\frac{45}{2}^-$ in the band. (a) Spectrum for the positive signature; gates were set on two transitions in list *a* and one in *c*. (b) Spectrum for the negative signature; gates were set on two transitions in list *b* and one in *c*.

The respective DCO ratios for the 555- ($\frac{15}{2}^- \rightarrow \frac{13}{2}^-$) and the 665-keV ($\frac{19}{2}^- \rightarrow \frac{17}{2}^-$) linking transitions are 0.58(9) and 0.55(8), in agreement with stretched dipole character. Between the spin values $\frac{21}{2}^-$ and $\frac{45}{2}^-$, the excited structure, Band 14, decays to the lower part of the signature *g* sequence in Band 13 via several transitions, for example, 693 ($\frac{41}{2}^- \rightarrow \frac{37}{2}^-$), 1370 ($\frac{21}{2}^- \rightarrow \frac{17}{2}^-$), and 1278 keV ($\frac{25}{2}^- \rightarrow \frac{21}{2}^-$). DCO ratios for four of these could be determined, and are consistent with stretched $E2$ character. Thus the spins and parity of this excited band could be verified.

The excitation energy of Band 13 was not known, but is now fixed by a number of linking transitions with other bands, which were presented earlier. These include two groups of stretched $E1$ feeding transitions: four from Band 8 and another four from Band 6. The band is also linked to Band 2 by several transitions at low and high spins. We note here an error in the initial work of Barnéoud and Foin [27] caused by incorrect placement of several low-energy transitions in the level scheme, where the $\frac{1}{2}^-$ level of the bandhead was placed 107.3 keV above the $\frac{1}{2}^+$ level of the Band 8 bandhead, and the $\frac{5}{2}^-$ level was placed 14.8 keV above the the $I = \frac{1}{2}^-$ bandhead. The correct energy of the $\frac{1}{2}^-$ level should be 136.5 keV above the $\frac{1}{2}^+$ level of Band 8, and the correct spacing between the $\frac{5}{2}^-$ and $\frac{1}{2}^-$ levels should be 19.6 keV. In such an arrangement, as shown in Fig. 3, Band 13 decays to Band 8 via the 225-, 107-, 103-, and 88-keV transitions.

6. Bands 15 and 16

Band 15 has been extended from $\frac{71}{2}^-$ to $(\frac{95}{2}^-)$, possibly $(\frac{97}{2}^-)$, based on the work of Yu *et al.* [28]. The band feeds the lowest two levels of Band 1, the ground-state band, via the 332-, 192-, and 294-keV γ rays, which can be seen in Fig. 3. Decays from Bands 2 and 4 to Band 15 have been discussed earlier. Coincidence spectra for Band 15 are shown in Fig. 14.

Band 16 feeds Band 15 at $\frac{31}{2}^-$ via a 677-keV γ ray, a transition which is an energy doublet in this decay sequence. Band 16 is also linked via the 614-keV ($\frac{43}{2}^- \rightarrow \frac{39}{2}^-$) γ ray from Band 13. Together, the 614-, 747-, and 677-keV γ rays change $6\hbar$ spin units. They are likely stretched $E2$ transitions, even though their DCO ratios could not be extracted. There is also a weak 752-keV transition from the 6659-keV level in Band 16 to the $\frac{49}{2}^-$ level in Band 13. The spins and parity of Band 16 above the $\frac{39}{2}^-$ level are undetermined. A coincidence spectrum for this band is shown in Fig. 10(c).

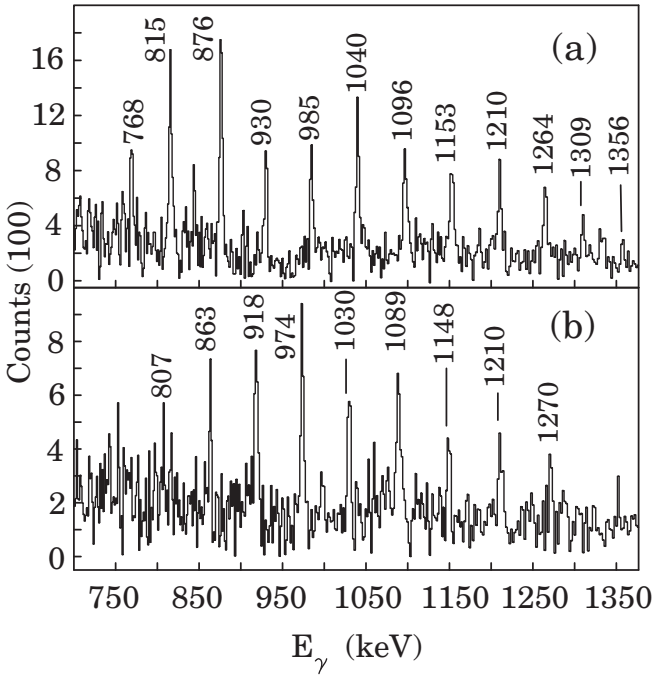

FIG. 15. Threefold coincidence spectra showing Bands 17 and 18. (a) Band 17: sum of double gates set on transitions in the band. It is not clear whether the unlabeled peak at 1334 keV is a continuation of the band at higher spin or a contamination from an unidentified source, since a consistent coincidence relationship between this γ ray and other band members could not be firmly established. (b) Band 18: sum of double gates set on transitions in the band.

7. Bands 17 and 18

Bands 17 and 18 are the weakest bands in the level scheme, with intensities less than 0.3% relative to the yrast band. Coincidence spectra for these bands are shown in Fig. 15. In both cases, clean gated spectra also show the transitions 212, 315, 411, and 498 keV (not shown in the figure), which all occur in Band 13 below the $\frac{25}{2}^-$ level. This fact suggests that Bands 17 and 18 must feed Band 13 above this level. However, definitive decay pathways between these bands and Band 13 could not be established. Therefore the spins, parity, and excitation energies of Bands 17 and 18 remain undetermined.

IV. INTERPRETATION OF BAND STRUCTURES

In order to interpret band structures in terms of intrinsic configurations and the underlying physics, we compared the observed dynamical properties of bands with the predictions of theoretical models. Theoretical quasiparticle Routhians were generated using the UC code [14,15], and are shown in Fig. 16. It was thus possible to compare the measured aligned angular momenta (alignments) and possible crossings of band structures with the theoretical values. Further interpretative constraints are provided by the excitation energies and energy splitting between signature partners. A systematic investigation of all the observed bands was carried out with respect to these observables. In Fig. 17 the experimental alignments of all the bands are displayed as a function of rotational

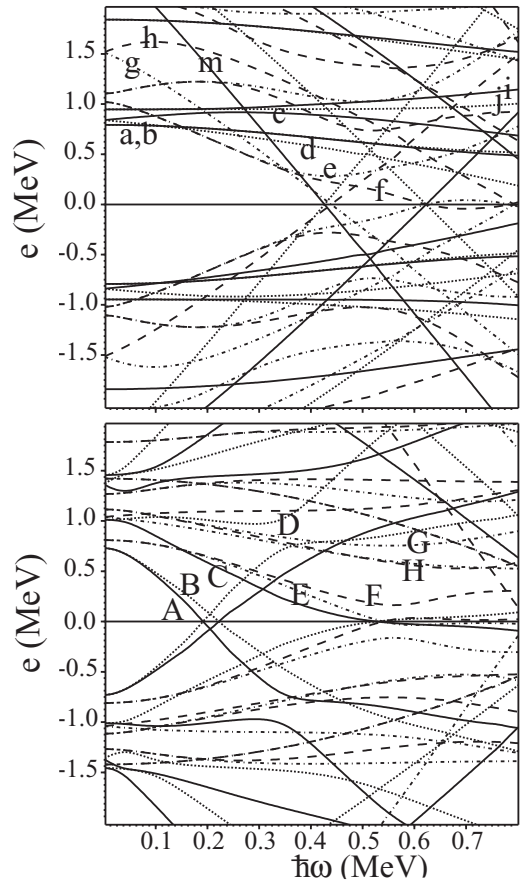

FIG. 16. Quasiparticle Routhians as a function of rotational frequency for protons (upper panel) and neutrons (lower panel), generated with the code ULTIMATE CRANKER [14,15] for ^{167}Lu for an axially symmetric potential with a quadrupole deformation of $\epsilon = 0.25$. Solid lines denote quasiparticle levels with $(\pi,\alpha) = (+,+\frac{1}{2})$, dotted lines denote $(+,-\frac{1}{2})$, dash-dotted lines denote $(-,+\frac{1}{2})$, and dashed lines $(-,-\frac{1}{2})$. Uppercase letters identify relevant neutron orbitals, and lowercase letters proton orbitals. The labeling convention is explained in Table II.

frequency. Figure 18 provides the excitation energies of all the bands relative to a rigid-rotor reference $AI(I+1)$, where the inertia parameter A was chosen to be 7.2 keV. The labeling of the quasiparticles and related orbitals closest to the Fermi surface is listed in Table II, where each letter corresponds to a state described by a given combination of asymptotic Nilsson orbitals and by appropriate signature (α) and parity quantum numbers. A summary of the assigned configurations and features of the band crossings is given in Table III.

A. Bands 1–4: $\pi[404]\frac{7}{2}^+$ and bands based on three-quasiparticle excitations

1. Band 1: a,b

Both the $\alpha = +\frac{1}{2}$ (a) and $\alpha = -\frac{1}{2}$ (b) sequences undergo a large alignment of $\sim 9.5\hbar$ at rotational frequency $\hbar\omega = 0.26$ MeV, as shown in Fig. 17(a). These values are consistent with those reported for this structure by Yu *et al.* [28], where

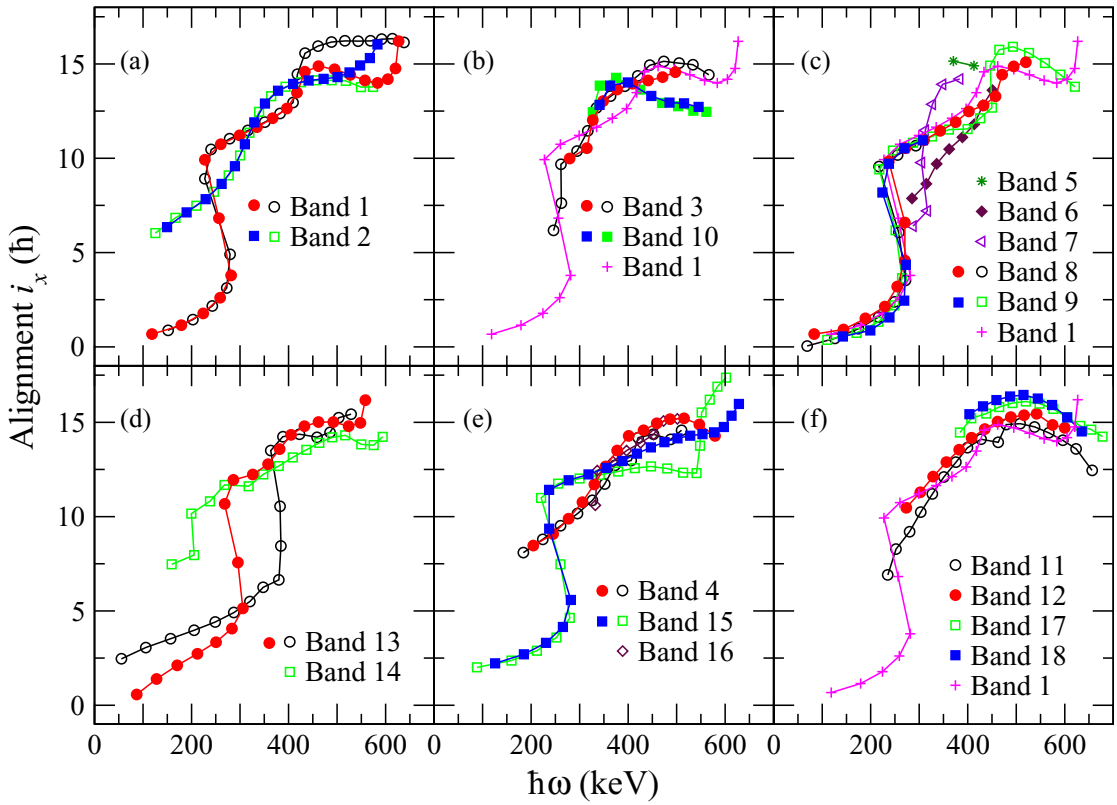

FIG. 17. (Color online) Aligned angular momenta for bands in ^{167}Lu, plotted as a function of the rotational frequency $\hbar\omega$. Open (closed) symbols represent the $\alpha = +\frac{1}{2}$ ($\alpha = -\frac{1}{2}$) sequences, except for Bands 17 and 18 whose signatures are not known and vertical positions are uncertain. The vertical position of Band 16 may be off by $1\hbar$ or so; see text for discussion. A reference with Harris parameters $J_0 = 27\ \hbar^2\text{MeV}^{-1}$ and $J_1 = 56\ \hbar^4\text{MeV}^{-3}$ was subtracted from the data. Band 1 is plotted in several selected panels for comparison.

the alignment gain was associated with the first $\nu i_{13/2}$ crossing, AB.

Although the subsequent sharp upbend shown by both signatures at 0.42 MeV [Fig. 17(a)] was attributed in Ref. [28] to the first proton alignment, ef, we consider that it is more likely due to the next available neutron crossing, CD. The argument is based on the *absence* of the CD crossing in alignment plots of positive-parity bands in the neighboring doubly odd nucleus, ^{168}Lu [30], which was also observed in our data. Those bands are built on the same $[404]\frac{7}{2}^+$ proton orbital coupled with the neutron orbital A, or the $[402]\frac{5}{2}^+$ proton coupled with the neutron orbital A. Thus the AB crossing is blocked in these bands. The first observed band crossing is BC, after which the next available crossing, CD, is expected to be blocked. None of the bands involving the A orbital in ^{168}Lu show any alignment gain around 0.4 MeV. However, if the up-bend in Band 1 (aAB,bAB) of ^{167}Lu at 0.42 MeV were indeed due to the ef crossing, then the ^{168}Lu aA,bA band should also show alignment at that frequency. We therefore attribute the up-bend in aAB,bAB in ^{167}Lu at 0.42 MeV to the CD crossing. The CD crossing has been observed elsewhere in this mass region, at a similar frequency. For example, the second band crossing at ∼0.4 MeV in positive-parity bands of ^{165}Lu has also been interpreted as CD [31]. An argument similar to that above was also used to interpret the second band crossing (at 0.37 MeV) in the ground-state band (based on $[402]\frac{5}{2}^+$) of the $N = 96$ isotonic neighbor, ^{169}Ta [32]. The two signatures achieve substantially different alignment gains in the CD crossing, with that of the positive signature being greater. The cause of this remains an open question.

Figure 17(a) also shows that the negative signature $bABCD$ then undergoes a further alignment at frequency ∼0.6 MeV, with a sharp up-bend, indicating a weak interaction. The quasiparticle Routhians generated by cranked shell model (CSM) calculations [see Fig. 16] suggest that the possible band crossings around this frequency are ef, fg, and EF. However, the predicted crossing frequency is strongly dependent on the strength of the pair field, which is likely to be strongly reduced after several band crossings. Further, the total alignment gain cannot be determined since a full alignment is not reached. In addition, the positive signature partner does not show a similar up-bend. If the up-bend involved the alignment of a pair of neutrons, it should be evident in both signatures. In the $N = 96$ isotone ^{168}Hf, only the proton fg crossing was reported above rotational frequencies of 0.5 MeV [26]. We therefore suggest that the high-frequency up-bend in this band may involve the alignment of protons.

2. *Band 2: aAE,bAE*

Inspecting the theoretical Routhians (Fig. 16) and the measured energies of the lowest one-quasiparticle excitations a,b and e, f (Fig. 3), one expects to find favorable excitations

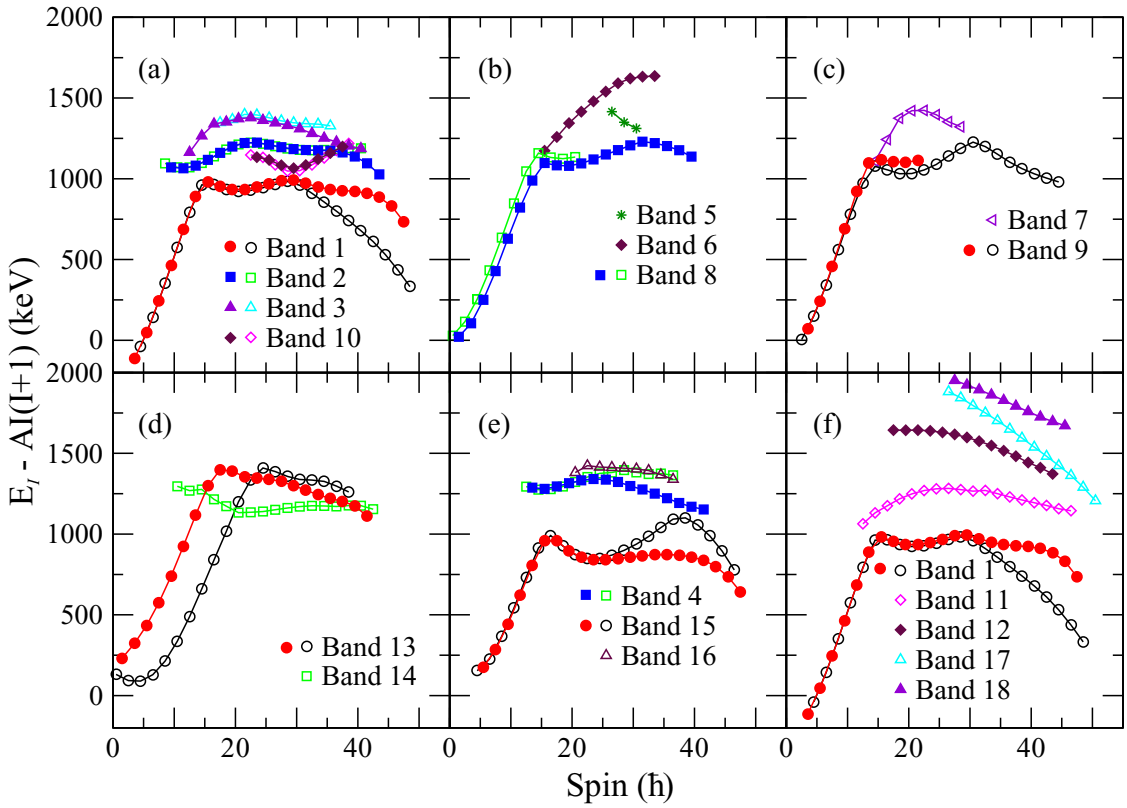

FIG. 18. (Color online) Excitation energies less a rigid rotor reference plotted versus spin for bands in ^{167}Lu. The inertia parameter $A = 7.2$ keV. Open (filled) symbols represent $\alpha = +\frac{1}{2}$ ($\alpha = -\frac{1}{2}$) sequences, except for Bands 17 and 18, where the signature is not known. The energies and spins of Bands 17 and 18 are uncertain, and the spins of Band 16 may be off by $1\hbar$ or so; see text for discussion.

of these coupled to the negative-parity two-quasiparticle excitations such as AE and AF, which are found in the doubly even neighbors. With the known signature splitting of the E and F orbitals being larger than that of the proton orbitals a,b and e,f, one expects negative-parity structures bAE,aAE and aAF,bAF, and likewise also positive-parity structures fAE,eAE and eAF,fAF, where each double pair is listed in order of increasing energy. The characteristic decay-out from, e.g., negative-parity aAE,bAE to positive-parity a or b is likely to be via $E1$ transitions, whereas $E2$ decay to the other negative-parity bands may occur, usually through the closeness of levels of identical spins. The expected band crossings in such three-quasiparticle structures are the BC neutron crossing, and possibly other higher-frequency unblocked crossings such as the ef or fg proton crossings. Such configurations are identified in Bands 2, 3, and 4.

TABLE II. Labeling of quasiparticle configurations and their Nilsson-orbital origins. Lowercase letters denote protons and uppercase letters neutrons. The spherical shell-model states represent only the main components of the wave functions if the orbitals are mixed.

Spherical shell model states	Nilsson orbital	$\alpha = +1/2$	$\alpha = -1/2$
$\pi g_{7/2}$	$[404]\frac{7}{2}^+$	a	b
$\pi d_{3/2}$	$[411]\frac{1}{2}^+$	c	d
$\pi d_{5/2}$	$[402]\frac{5}{2}^+$	i	j
$\pi i_{13/2}$	$[660]\frac{1}{2}^+$	m	
$\pi h_{11/2}$	$[514]\frac{9}{2}^-$	e	f
$\pi h_{9/2}$	$[541]\frac{1}{2}^-$	g	h
$\nu i_{13/2}$	$[642]\frac{5}{2}^+$	A	B
$\nu i_{13/2}$	$[651]\frac{3}{2}^+$	C	D
$\nu f_{7/2}$	$[523]\frac{5}{2}^-$	E	F
$\nu h_{9/2}$	$[521]\frac{3}{2}^-$	G	H

The large excitation energy (~1 MeV) of the bottom of Band 2, shown in Fig. 18(a), is consistent with a three-quasiparticle structure. Band 2 has a negative parity. Considering that this band decays to Band 1, its structure would most likely involve one of the a,b orbitals coupled to the negative-parity neutron configuration AE or AF. Such bands have also been observed in several neighboring nuclei. Two likely configurations would thus be aAE,aAF and aAE,bAE. The energy splitting of the two signatures is compared with CSM predictions in order to choose between these alternatives. The upper panel of Fig. 16 shows that the Routhians a,b are expected to remain degenerate up to high rotational frequencies (~0.6 MeV), whereas E,F (lower panel, same figure) are predicted to show large splitting above 0.2 MeV, with E rapidly becoming energetically favored. However, the measured excitation energies of the

TABLE III. Observed band crossings in ^{167}Lu. i_x denotes the aligned angular momentum. For the one-quasiparticle bands, i_x was extracted at $\hbar\omega \simeq 0.2$ MeV.

Band	Configuration	Initial i_x ($\hbar$)	Crossings	$\hbar\omega_c$ (MeV)	Expt. Δi_x ($\hbar$)
Band 1	a,b	0.5	AB	0.26	9.5
	aAB		CD	0.42	5.0
	bAB		CD	0.42	4.0
	$bABCD$		proton	0.62	>2.5
Band 2	aAE,bAE	6.0	BC	0.32	8.0
	$aAEBC$		ef (?)	∼0.5	>2
Band 3	aAF,bAF	∼10	BC	∼0.32	>4
Band 4	eAF,fAF	8.0	BC	∼0.32	6.5
Band 5	$cBCAD$				
Band 6	γ vibration				
Band 7	iBC	5.5	AD	0.32	∼8
Band 8	c,d	∼0	AB	0.27	10
	dAB		CD	0.46	∼5
Band 9	i,j	0.5	AB	0.25	10
	iAB		CD	0.46	5.0
Band 10	$aABCD$,$bABCD$	12.5	→ aAB,bAB	0.45	
Band 11	TSD1 (0-phonon)				
Band 12	TSD2 (1-phonon)				
Band 13	g	2.5	BC+AD	0.38	9
	h	0.5	AB	0.29	8
	hAB		CD	0.4–0.5	∼6
	$hABCD$		proton	0.55	>1
Band 14	gAB		CD/EF	0.4–0.5	
	$gAB(CD/EF)$		ef	∼0.57	
Band 15	e,f	2.0	AB	0.26	10
	fAB		CD	0.35–0.55	∼2
	$fABCD$		EF	0.6	>2
	eAB		fg	0.55	>5
Band 16	eBC	∼12	AD	0.35–0.50	∼2.5
Band 17	TSD(?)				
Band 18	TSD(?)				

two signatures in Band 2, shown in Fig. 18(a), remain nearly degenerate until spins higher than 35$\hbar$. These considerations make aAE,bAE the more likely configuration for Band 2. This suggestion is consistent with the following considerations: (1) The initial alignment [Fig. 17(a)] of $i_x \simeq 6\hbar$ relative to a,b is approximately equal to the sum of contributions from the participant proton and neutrons: $i_x(a) + i_x(A) + i_x(E) = (0 + 5.5 + 1.8)\hbar = 7.3\hbar$. (2) The alignment gain $\Delta i_x \simeq 8\hbar$, and also the shape of the up-bend at 0.32 MeV [Fig. 17(a)], both suggest a BC crossing. Above the up-bend the configuration therefore involves five quasiparticles, $aAEBC$ and $bAEBC$. (3) Bands built on the AE configuration have been reported in the doubly even neighbors ^{166}Hf [33] and ^{168}Hf [26], and in odd-Z neighbors ^{165}Lu [31] and ^{165}Tm [34] as well. These structures all show the BC crossing.

At rotational frequencies above 0.5 MeV the negative signature $aAEBC$ exhibits the onset of a further alignment gain, shown in Fig. 17(a). The exact crossing frequencies cannot be established because the band does not extend to sufficiently high spins. Our UC calculations, shown in Fig. 16, predict four possible band crossings in the frequency range 0.4–0.6 MeV: CD, EF, ef, and fg. In this case the CD and EF neutron crossings are expected to be Pauli blocked since the band involves both the E and C orbitals. The remaining candidates are therefore the proton crossings. The ef crossing is calculated to occur at the rotational frequency 0.42 MeV, and has been reported in the $[402]\frac{5}{2}^+$ band in the $N = 98$ nucleus ^{171}Ta [35] at this frequency. The predicted alignment gain is ∼3$\hbar$. The fg crossing is predicted at 0.48 MeV, with a larger alignment gain of ∼5.5$\hbar$. It has been reported at 0.55 MeV with this alignment gain in several bands in the $N = 96$ isotone ^{168}Hf [26]. Because we do not observe all the features of the up-bend in Band 2, and because the predicted crossing frequencies are parameter dependent, we restrict ourselves to the suggestion that this up-bend is likely associated with either the ef or the fg crossing.

3. Band 3: aAF,bAF

It is evident from the measured alignments [Fig. 17(b)] and excitation energies [Fig. 18(a)] that the larger part of Band 3 behaves as a pair of signature partners. This is certainly true above spin $\frac{33}{2}$, below which the alignment pattern is irregular. The initial alignment of ∼10$\hbar$ (measured at $\hbar\omega \simeq 0.3$ MeV) is indicative of a three-quasiparticle character, since such a large alignment cannot be generated by any one of the proton

orbitals near the Fermi surface. Further, Fig. 17(b) shows that the band undergoes a smooth BC crossing at ∼0.34 MeV. The intrinsic structure must therefore exclude the B neutron orbital, or the crossing would be blocked. This leaves the energetically favorable AE or AF neutron configurations as the most likely candidates. The respective alignment contributions of the orbitals A, E, and F are 5.5$\hbar$, 1.8$\hbar$, and 1.5$\hbar$ [26]. Either one of the above suggested configurations would account for the full measured initial alignment, and would have to be coupled with a positive-parity proton orbital with roughly zero alignment in order to make a three-quasiparticle structure. In fact the Nilsson orbitals $\pi[404]\frac{7}{2}^+$, $\pi[411]\frac{1}{2}^+$, and $\pi[402]\frac{5}{2}^+$ all satisfy these requirements, the first (a,b) being energetically most favored. The configuration aAE,bAE has already been assigned to Band 2. We therefore assign the intrinsic structure aAF,bAF to Band 3.

Several considerations support this assignment. First, it is very likely that the observation of the structure aAE,bAE in our data would be accompanied by the observation of aAF,bAF, given that the splitting between the orbitals E and F is not very large. Second, the excitation energy plot [Fig. 18(a)] shows that the proposed aAF,bAF configuration (Band 3) lies higher in energy than aAE,bAE (Band 2). Third, the excitation energy plot also shows that Band 3 exhibits almost zero splitting below spin $I \sim 30$. The splitting at higher spins is due to the $[404]7/2^+$ proton orbital, and such behavior is consistent with a large K projection. The bottom part of the positive signature exhibits an irregular alignment pattern and a lower excitation energy than the rest of the band. Similar behavior is exhibited by the band BE in ^{168}Hf [26], and was attributed to mixing with an octupole vibration [36], which causes a lowering of the energy.

4. Band 4: eAF, fAF

The excitation energies of Band 4 [Fig. 18(e)] clearly show Band 4 to be a three-quasiparticle structure at low spins: it lies some 300 keV above Band 15 (configurations eAB and fAB). The alignments of Band 4 [Fig. 17(e)] show a BC crossing, similar to the bands aAE,bAE and aAF,bAF. It must therefore involve the neutron orbital A. The alignments are similar to those of Band 15 (which involves e,f), in that they exhibit a large signature splitting, with the negative signature undergoing a larger alignment gain. This suggests that a possible configuration may be either eAE,fAE, or eAF,fAF. Since the negative signature f of Band 15 has a lower excitation energy and a larger alignment gain than the positive signature e, the negative signature of Band 4 should involve the f orbital (rather than e). Thus the most likely configuration is fAF. The positive signature is then eAF. Further, over most of the observed spin range, Band 4 has a lower excitation energy than Band 3 (aAF,bAF). This is consistent with the fact that the calculated e,f Routhians are energetically lower than a,b; see Fig. 16.

We also considered an alternative scenario, in which the negative (positive) signature may correspond to eAE (fAE). However, with such an interpretation eAE would show greater alignment and smaller excitation energy than fAE, both of which are inconsistent with the known properties of the e,f orbitals. In addition, the excitation energy of Band 4 is ∼100 keV higher than that of Band 2 (aAE,bAE), in conflict with the e,f orbitals having lower energy than a,b, as mentioned above. Hence the alternative suggestion is extremely unlikely. The relative excitation energy of these two bands can be accounted for if Band 4 involves the neutron orbital F instead of E, because F becomes energetically unfavored at rotational frequencies above ∼200 keV. This is consistent with the eAF,fAF interpretation.

It should be mentioned that, although the band eAE,fAE is expected to have a lower excitation energy than eAF,fAF, no such band was observed in our data. The mystery of the "missing" eAE,fAE band remains an open question. It is possible that not all of these weak bands have been identified.

The alignments plotted in Fig. 17(e) show that, at $\hbar\omega \sim$ 0.2 MeV, Band 4 is ∼1.5$\hbar$ more aligned than Band 2 [Fig. 17(a)]. Since the proposed configuration aAE,bAE for Band 2 differs only with respect to the participating proton, the alignment offset should reflect relevant differences between the e,f and a,b orbitals. This is found to be the case. Table III records that the measured alignment of e,f is 1.7$\hbar$ more than a,b, very close to the observed difference between the relevant three-quasiparticle bands. Band 4 undergoes further alignment above 0.3 MeV. The alignment pattern and the gain of ∼6.5$\hbar$ are consistent with a BC crossing. The upper part of the band is therefore proposed to be the five-quasiparticle structure $eAFBC,fAFBC$. The irregularity in the alignment curve of the positive signature eAF is likely caused by its interaction with Band 5.

The negative signature (fAF) was reported in Ref. [23] as a decoupled band, and was suggested there that the band may be a candidate TSD band with negative parity. The claimed large deformation of the band was inferred from its large dynamical moment of inertia, $J^{(2)}$, and preliminary results from lifetime measurements of the transition quadrupole moments Q_t. It is now clear that the sequence is a signature partner of a coupled band with positive parity. In addition, the hint of a larger Q_t moment could not be confirmed in the later analysis [37]. A large $J^{(2)}$ moment alone is not a solid proof of large deformation. A closer inspection of the $J^{(2)}$ plot of Band 4 indicates that the large average $J^{(2)}$ value is mainly caused by a broad bump between rotational frequencies 250 and 420 keV. The bump corresponds to the observed gradual increase of aligned angular momentum of the band associated with the BC crossing. Thus, the the interpretation of the sequence being a TSD band in our original publication [23] is incorrect.

B. Bands 5–10: $\pi[411]\frac{1}{2}^+$, $\pi[402]\frac{5}{2}^+$, and side bands

1. Band 8: c,d

The measured dynamical properties of this band are consistent with the tentative configuration assignment made by Yu *et al.* [28]. For example, the large signature splitting of this band, visible in the experimental excitation energy plot [Fig. 18(b)], is to be expected of a low-K structure. Further, the alignment pattern [Fig. 17(c)] is similar to that exhibited by the $[411]\frac{1}{2}^+$ structures in the neighboring nuclei, ^{165}Lu ($N = 94$) [31], ^{169}Ta ($N = 96$) [32], and ^{171}Ta ($N = 98$) [35],

where it was given the same interpretation. In all cases the favored signature is substantially more aligned than the unfavored partner before the AB crossing. At low spins the band mixes strongly with the configuration $[402]\frac{5}{2}^+$ (Band 9). The AB crossing at 0.27 MeV raises the alignment of both signatures by $\sim 10\hbar$. Above this crossing, the cAB sequence continues as the positive signature partner of Band 10. The partner, dAB, undergoes a further gradual alignment gain of $\sim 5\hbar$ in the frequency range 0.35–0.52 MeV. A local maximum in the plot of the dynamic moments of inertia $J^{(2)}$ (not shown) suggests a crossing frequency of 0.46 MeV. This is attributed to the CD crossing, using the argument presented in Sec. IV A for Band 1.

An interesting finding is the existence of a series of $E1$ γ rays decaying from Band 8 to Band 13. A similar occurrence of low-energy electrical dipole transitions between the $\pi[411]\frac{1}{2}^+$ and the $\pi[541]\frac{1}{2}^-$ bands has been observed in a number of odd-A rare-earth nuclei, e.g., ^{165}Tm [34], ^{169}Lu [38], ^{171}Lu [39], and ^{173}Ta [40] where an enhanced $E1$ strength was found systematically. The enhancement has been analyzed by Hagemann *et al.* [41] in terms of a coupling to octupole vibrational degrees of freedom for the core.

2. Band 9: i, j

The band associated with the i, j proton orbitals was previously identified in the earlier work of Yu *et al.* [28]. The low-spin part of the band contains a strong $[411]\frac{1}{2}^+$ admixture, deduced from the numerous decays between it and Band 8. Interestingly, in the $N = 96$ isotone ^{169}Ta, the configuration $[402]\frac{5}{2}^+$ is reported to mix strongly with $[404]\frac{7}{2}^+$, based on the measured $B(M1)/B(E2)$ ratios [32], rather than with $[411]\frac{1}{2}^+$. Unsurprisingly, there is also considerable crosstalk between the two mixed bands in that nucleus. In ^{167}Lu, both signatures undergo an AB crossing with an alignment gain of $\Delta i_x \simeq 10\hbar$ at 0.25 MeV, as shown in Fig. 17(c). The jAB sequence persists at higher frequencies, where it forms one partner of Band 10. The iAB sequence shows a sharp up-bend with a gain of $\sim 5\hbar$ at 0.46 MeV. Using the argument presented in Sec. IV A for Band 1, we attribute this to the CD crossing. The CD crossing was also associated with an up-bend in the $[402]\frac{5}{2}^+$ band of ^{169}Ta, although at somewhat lower rotational frequency (0.37 MeV) [32].

3. Band 10: A Landau-Zener crossing

Although the two signatures of Band 10 mainly feed the signatures c in Band 8 and j in Band 9, Band 10 is *not* the high-spin continuation of these bands. Band 10 displays a further alignment gain at $\hbar\omega \sim 0.34$ MeV which is not exhibited by Bands 8 and 9; see Figs. 17(b) and 17(c). This indicates that Band 10 has a different configuration from the latter two bands. It can be further observed in Fig. 18(a) that the excitation energies of Bands 1 and 10 are nearly degenerate at spin $\frac{57}{2}$. These bands exchange character at that point. At spins above $\frac{57}{2}$ Band 10 is the continuation of the three-quasiparticle structures aAB,bAB (Band 1), while the lower part of Band 10 is the low-spin extension of the five-quasiparticle structure $aABCD$,$bABCD$. Such exchanges of intrinsic structure between bands, a Landau-Zener crossing [42], have been documented elsewhere, such as that between Bands 3 and 6 in ^{168}Hf [26]. Bands 1 and 10 interact strongly. An upper limit for the interaction strength, equal to half the energy difference between the bands at the point of closest approach, is $|V_{\max}| \simeq 33$ keV. A consequence of mixing between Band 1 and Band 10 is the presence of several linking $E2$ transitions, between spin values of $\frac{49}{2}$ and $\frac{61}{2}$. Additional support for our configuration assignment can be obtained by comparing the aligned angular momenta of Bands 7 and 10. Both bands have $\sim 14.2\hbar$ alignment in a region of $0.35 < \hbar\omega < 0.4$ MeV where Bands 7 and 10 have configurations $iBCAD$ and $aABCD$, respectively. The aligned angular momenta in both bands are from orbitals $ABCD$ because the contributions from orbitals a and i are negligible.

4. Band 6: γ vibration

This positive-parity band decays from the $\frac{35}{2}$ and $\frac{31}{2}$ levels to Band 8 with stretched $E2$ γ rays. We did not observe a signature partner band. The alignment pattern [Fig. 17(c)] and excitation energy [Fig. 18(b)] differ from those of the remaining ND bands. For example, the band does not undergo any of the expected band crossings exhibited by the other bands. The initial alignment of $\sim 7.5\hbar$ exceeds that of the most aligned one-quasiparticle band (g) by some $5\hbar$, but is less than that of any of the other three-quasiparticle bands, even though the excitation energy has an initial value (~ 1.2 MeV) comparable to that of other three-quasiparticle bands. The excitation energy plot shows an anomalous pattern at high spins: the positive slope contrasts with the flat profile of the other ND bands. In fact, it looks like an extension of that of the signature d of Band 8, but with a slightly higher energy. Furthermore, there are four $E1$ transitions decaying from lower-spin levels in Band 6, between $\frac{43}{2}$ and $\frac{31}{2}$, to Band 13, similar to what occurs in the signature d between levels $\frac{31}{2}$ and $\frac{15}{2}$, indicating that the Band 6 could have an intrinsic structure resembling that of signature d. It is thus plausible to suggest that Band 6 is a γ-vibrational band built on Band 8, the $\pi[411]\frac{1}{2}^+$ orbital.

5. Bands 7 and 5: $iBC \rightarrow iBCAD$ and $cBCAD$

In order to suggest a configuration for Band 7, the excitation energies were compared with those of Band 9 ($i \rightarrow iAB \rightarrow iABCD$), as shown in Fig. 18(c). It is evident that, at low spins, Band 7 appears to be continuation of the positive signature of Band 9, and that it approaches Band 9 again at higher spins. The initial alignment [$\sim 5.5\hbar$, see Fig. 17(c)] suggests an initial three-quasiparticle structure for this band, even though it does not start from a fully aligned configuration. The sharp up-bend at $\hbar\omega \approx 0.32$ MeV reaches a total alignment gain of $14.2\hbar$, indicating a five-quasiparticle structure at high spins, approaching the upper part of Band 9. We suggest that the up-bend is the BC crossing followed immediately by the AD crossing. Therefore, Band 7 involves the quasiparticle configuration $iBCAD$, and is the low-spin extension of the upper part of Band 9 ($iABCD$ configuration), which decays either along the main sequence of the band to the iAB

configuration and then to the single-quasiparticle configuration i, or through Band 7 to the configuration iBC and finally to Band 1.

Band 5 consists of only three levels, which makes a definitive configuration assignment difficult. The band interacts with Bands 11 and 12 (TSD structures). Its excitation energies are similar to those of Band 7 [Figs. 18(b) and 18(c)], and its alignment is $0.5\hbar$ higher than the full alignment gain of the $iBCAD$ configuration in Band 7 [Fig. 17(c)]. A speculative suggestion for this short sequence may be $cBCAD$.

C. Bands 11 and 12: The wobbling excitations

The positive-parity bands Band 11 and Band 12 are discussed in some detail in Ref. [5], where they are described as triaxial strongly deformed bands TSD1 and TSD2. In summary, Band 11 (TSD1) was associated with the favored $\alpha = +\frac{1}{2}$ signature of the $\pi i_{13/2}$, $[660]\frac{1}{2}^+$ orbital, and Band 12 (TSD2) with the one-phonon wobbling excitation of the same configuration. They were identified as excitations in the triaxial deformed potential energy minimum predicted by UC calculations to occur at $(\epsilon,\gamma) \sim (0.4, 20^\circ)$.

It is interesting to note the new decay from $\frac{65}{2}^+$ of Band 11 to $\frac{61}{2}^+$ of Band 5 via an 880-keV γ ray. This establishes the interaction of TSD1 and two ND bands, *viz.* Band 9 ($iABCD$) and Band 5 (tentatively $cBCAD$), and also the mixing of the $\frac{61}{2}^+$ levels of these three bands. Previously, it was a puzzle why the energy of the $\frac{61}{2}^+$ level in Band 11 was so low when considering only the interaction between Bands 11 and 9. It is now clear that this level is pushed down by the $\frac{61}{2}^+$ level of Band 5.

D. Bands 13 and 14: $\pi[541]\frac{1}{2}^-$ and side band

1. *Band 13: g,h*

$K = \frac{1}{2}$ bands are known to exhibit pronounced splitting between the favored and unfavored signatures, even at the lowest rotational frequencies. Such a large splitting is apparent, for this band, in the excitation energy plot [Fig. 18(d)]. There is thus no doubt that the present negative-parity band has a low K projection, and must therefore be associated with the lowest-energy negative-parity aligned proton orbital, namely $\pi[541]\frac{1}{2}^-$. This is in agreement with the previous assignment of Yu *et al.* [28]. Rotational structures built on this deformation-driving proton orbital are observed systematically in the rare-earth nuclei. Examples are found in the $Z = 71$ nuclei ^{165}Lu [31], ^{167}Lu [28], ^{169}Lu [38], ^{171}Lu [39], and also in several $Z = 73$ nuclei ^{167}Ta [43], ^{169}Ta [32], and ^{171}Ta [35]. Interestingly, they were not observed in the $N = 92$ isotones ^{163}Lu [9] and ^{165}Ta [44]. This is consistent with the experimental observation and theoretical predictions that the bandhead energy of the $\pi[541]\frac{1}{2}^-$ bands in the Ta isotopes has a local minimum at $N = 100$, below which it increases with decreasing neutron number [32]. The same trend may be expected in the Lu isotopes.

In some respects, $\pi[541]\frac{1}{2}^-$ bands exhibit several unique features when compared with the other ND bands, such as a larger deformation, larger initial alignment before the AB neutron crossing (corresponding to the larger slope of orbital g in Fig. 16), smaller alignment gain, and a signature-dependent delayed AB crossing frequency, with the favored ($\alpha = +\frac{1}{2}$) sequence exhibiting the greater delay. The latter is not adequately explained by CSM calculations if only enhanced deformation is considered, and it has been suggested that the behavior may be attributed in part to a signature-dependent pn interaction [32].

Band 13 exhibits all of these features, some of which may be seen in the alignment plot [Fig. 17(d)]. We first consider the behavior of the favored sequence g. This one-quasiparticle sequence is seen to undergo a sharp alignment at $\hbar\omega_c = 0.38$ MeV with a gain of $9\hbar$. Our data show the full evolution of the band crossing for the first time. Yu *et al.* [28] suggested that the large alignment gain be explained by the alignment of four quasineutrons, namely a BC crossing followed closely by AD. We agree with this suggestion. Indeed, these crossings are expected at similar frequencies, respectively ~0.31 MeV and ~0.34 MeV, according to UC calculations (Fig. 16). Therefore the configuration of the band after the crossing is proposed to be $gBCAD$. Further support for this suggestion is the absence of the CD crossing in this band, which is blocked by the participation of the C and D neutrons. If the alignment plot for this band is compared with that of band hAB (discussed below) in the region 0.4–0.5 MeV, the absence of further alignment gain is apparent.

Turning now from the favored to the unfavored sequence h, the lowest-frequency up-bend at 0.29 MeV [Fig. 17(d)] is interpreted as $h \rightarrow hAB$. The gradual increase in alignment in the region 0.4–0.5 MeV is attributed to the CD crossing. After this crossing, the $hABCD$ band shows a sharp up-bend observed at 0.55 MeV, probably due to a proton crossing.

2. *Band 14: gAB → gABCD*

The g orbital undergoes an AB crossing at $\hbar\omega \sim 0.34$ MeV, and continues upward as Band 14. This is more apparent if the upper part (above $\frac{41}{2}^-$) of Band 14 is plotted as the high-spin continuation of g, as shown in Fig. 17(d). The crossing is substantially delayed compared with the AB crossing at ~260 keV seen in Bands 1 and 15. Thus Band 14 has the configuration gAB, consistent with the band having $\sim 1.5\hbar$ (extracted at $\hbar\omega \sim 0.4$ MeV) less alignment than Band 13, $gBCAD$; see Fig. 17(d). This three-quasiparticle configuration extends down to spin 21/2. There is a gradual alignment increase of $\sim 2\hbar$ over the region 0.4–0.5 MeV. Similar behavior is exhibited by Band AB of ^{166}Hf [33] and ^{168}Hf [26], which was attributed to either the neutron CD alignment or to a mixture of CD and EF alignments with a strong interaction. The latter interpretation seems more probable for Band 14 here since a pure CD crossing would make the upper part of the band $gABCD$, duplicating the configuration of Band 13. At ~0.57 MeV, this sequence shows the onset of further alignment, probably due to a proton crossing.

E. Bands 15 and 16: $\pi[514]\frac{9}{2}^-$ and side-band

1. Band 15: e, f

Band 15 exhibits well-known behavior in this mass region. For example, the alignments [Fig. 17(e)] show the characteristic backbend associated with the AB crossing, at the frequency $\hbar\omega_c = 0.26$ MeV and with alignment gain $\Delta i_x \simeq 10\hbar$. These values are similar to those reported by Yu *et al.* [28]. At higher rotational frequencies the alignment pattern is similar to that of $[514]\frac{9}{2}^-$ bands in other odd-A rare-earth nuclei such as ^{165}Lu [31], ^{169}Ta [32], and ^{171}Ta [35]. In these cases both signatures undergo a gradual increase in alignment above the AB crossing, with the negative signature experiencing the greater increase. In ^{167}Lu this difference is more pronounced, however: from $\hbar\omega \simeq 0.3$ MeV until 0.55 MeV the positive signature eAB shows no further gain while the negative signature gains a further $2\hbar$. Aspects of this behavior are predicted by UC calculations (Fig. 16). These anticipate large signature splitting between the e and f protons, above ∼0.4 MeV, resulting in different alignments for the eAB and fAB sequences. The excitation energies [Fig. 18(e)] also show such a splitting. In the isotone ^{169}Ta the gradual alignment gain in the region of $\hbar\omega \sim 0.4$ MeV was associated with the CD crossing [32]. We therefore attribute this gradual alignment gain in the fAB sequence of ^{167}Lu to the CD neutron crossing. Why such a crossing is observed in one signature and not the other remains an open question. Aspects of the CD crossing, such as its apparent absence from the $N = 96$ isotone ^{168}Hf [26], and from the $N = 98$ nuclei ^{170}Hf [45] and ^{171}Ta [35], are not well understood.

The sharp alignment gain of $\sim 5\hbar$ exhibited by the eAB sequence at 0.55 MeV shares many characteristics with the proton fg mixed crossing observed in three bands in the isotone ^{168}Hf [26]. In those bands, the measured crossing frequency was 0.55 MeV and the alignment gain $\sim 5\hbar$. Indeed, the ef crossing is expected to be blocked in both signature partners, while the fg crossing is expected to be blocked in the negative signature partner f (where the up-bend is entirely absent), but not the positive partner. Crossings involving neutrons or different proton orbitals would be expected to manifest as up-bends in *both* partners. The most compelling suggestion is therefore that this up-bend is associated with the fg crossing.

At still higher frequencies (∼0.6 MeV) the $fABCD$ sequence has an alignment gain of $\sim 2\hbar$. UC calculations predict likely crossings to be the mixed crossing $\pi i_{13/2}g_{7/2}$ (mb) and $\nu f_{7/2}$ (EF). The first of these crossings, mb, involves the highly aligned $\pi[660]\frac{1}{2}^+$ and the $\pi[404]\frac{7}{2}^+$ orbitals, and is expected to contribute an alignment gain of $\sim 5\hbar$ [46]. The EF crossing is expected to contribute a gain of $\sim 3\hbar$ [46], and is thus more consistent with the modest gain observed in this band. Support for this suggestion is that an EF alignment at a similar frequency was reported for the $\pi[514]\frac{9}{2}^-$ band in neighboring ^{165}Lu [31]. We therefore suggest that the negative signature sequence undergoes an EF crossing, and ends up with an impressive seven-quasiparticle configuration, $fABCDEF$.

2. Band 16: eBC

The spins and parity of Band 16 above the $\frac{39}{2}^-$ level are undetermined. The band is plotted in Fig. 17 and 18 with an assumption that all transitions above the $\frac{39}{2}^-$ level, including the 752-keV linking transition to Band 13, are stretched $E2$'s. If the 752-keV γ ray changes angular momentum by $\Delta I = 1\hbar$, the level spins in Band 16 will be lower than the assumed values by $1\hbar$. Band 16 is possibly an extension of Band 15 (e, f). The alignment plot [Fig. 17(e)] shows that the band is more aligned than fAB. We suggest that Band 16 is likely eBC which then undergoes the AD alignment, similar to Band 13 ($gBCAD$).

F. Bands 17 and 18: TSD bands built on quasiparticle excitations?

Figure 19 shows the dynamical moments of inertia $J^{(2)}$ of Bands 17 and 18, together with those of an ND band (Band 15) and the wobbling band TSD2 (Band 12). It is evident from the figure that the average $J^{(2)}$ values of Bands 17 and 18 are ∼20% higher than those of the ND band, but are similar to those of TSD2. While large $J^{(2)}$ values are often taken as a possible indication of large deformation, band crossings associated with strong interactions can produce broad bumps in $J^{(2)}$ plots, resulting in large average $J^{(2)}$ values. Caution must be exercised to avoid mistake similar to that for Band 4 in Ref. [23], as discussed earlier. The $J^{(2)}$ plots of Bands 17 and 18 are rather smooth and flat, except for Band 17 at the lowest and highest rotational frequencies. Furthermore, no sign of band crossings is observed in the alignment plots (Fig. 17) and the excitation energies (Fig. 18) of the two bands. Therefore,

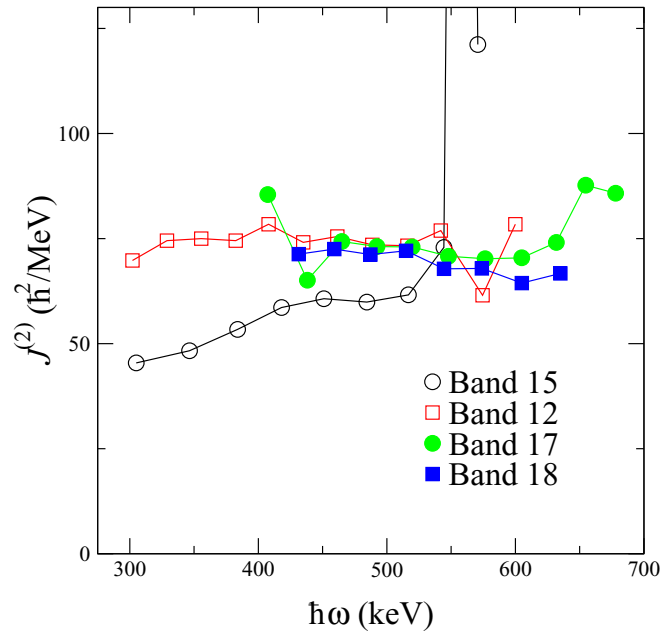

FIG. 19. (Color online) Dynamic moments of inertia, $J^{(2)}$, for the presumed TSD bands, Bands 17 and 18, in ^{167}Lu. Those of the positive signature of the ND Band 15 and wobbling Band 12 are shown for comparison. The large spike at the highest spins for Band 15 corresponds to the proton crossing.

Bands 17, 18, and TSD2 may have similar deformation and share some similar properties.

The spins and parity of Bands 17 and 18 are indeterminate since no linking transitions to the known structures could be established. Considering their low population intensity of less than ∼0.3% relative to the yrast sequence, these two bands likely have higher excitation energies than TSD1 and TSD2 (Bands 11 and 12). A rough estimate of the spins was made to obtain reasonable alignments when compared to TSD1 and TSD2, and to the ND structures. Thus the positions of Bands 17 and 18 in Fig. 18(f) are uncertain. However, the spin uncertainty affects only their vertical but not the horizontal positions in the alignment plot Fig. 17(f); the alignment pattern remains unaffected. Figure 17(f) shows that the bands do not exhibit any signs of band crossings between rotational frequencies 0.35 and 0.67 MeV, especially the proton alignment for ND bands at frequencies 0.55–0.6 MeV. In this respect too, Bands 11, 12, 17, and 18 form a group distinct from the ND bands. This may suggest that the proton intruder orbitals have already been occupied at lower spins in the bands, and that the bands are associated with the TSD potential energy minimum, rather than the ND minimum.

Bands 11 and 12 decay to positive-parity Bands 8 and 9; Bands 17 and 18 feed the negative-parity Band 13. The four bands cannot be in the same wobbling family. No linking transitions between Bands 17 and 18 could be identified; it is unknown whether the two bands are based on a wobbling excitation. On the other hand, judging from the estimated alignments and excitations, the bands contain at least three quasiparticles. TSD bands based on multiquasiparticle excitations have been identified in several neighboring nuclei; for example, TSD4 in ^{163}Lu with a configuration of $\pi i_{13/2} \otimes \nu(i_{13/2}h_{9/2})$ [9] and the TSD bands in ^{164}Lu with configurations of $\pi i_{13/2} \otimes \nu h_{9/2}$ or $\pi i_{13/2} \otimes \nu i_{13/2}$ [10]. TSD bands with similar configurations may thus also exist in ^{167}Lu.

V. SUMMARY

The present work has presented the most complete high spin spectroscopic investigation of the nucleus ^{167}Lu to date. Previously observed [28] rotational bands have been extended up to much higher spins, and supplemented with ten new rotational bands. A large number of interband linking transitions at medium- and high-spin region were identified so that all but two bands could be connected with each other, and the energies of all bandheads have been determined. A number of band interactions, including a Landau-Zener crossing, were observed. Configurations were proposed for all new bands based on measured observables, with the help of cranked shell model calculations. At low spins the $[411]\frac{1}{2}^+$ and $[402]\frac{5}{2}^+$ configurations are strongly mixed. The $E1$ transitions between the $[411]\frac{1}{2}^+$ and $[541]\frac{1}{2}^-$ bands, that have been observed systematically in neighboring odd-A rare-earth nuclei, are likely octupole enhanced. Several three-quasiparticle bands involving the AE or AF neutron pair are observed to become energetically competitive. Five-quasiparticle excitations were observed in most bands. The detailed spectroscopy puts our study of TSD structures in ^{167}Lu on a solid footing. Bands 11 and 12 constitute a family of wobbling bands, which is a unique fingerprint of triaxiality. An interesting phenomenon is the mixing of states in the ND and TSD potential wells, viz., the three-band interaction between Bands 11, 5, and 9 around spin $\frac{61}{2}^+$. A γ-ray sequence, previously suggested as a TSD band based on quasiparticle excitations, has now been determined to be a signature partner of a coupled band, associated with a normal deformed five-quasiparticle configuration. Two new bands, Bands 17 and 18, could not be linked to the ND states. They are found to have large dynamical moments of inertia, a possible indication of larger deformation, and an alignment pattern similar to that of bands TSD1 and TSD2. Further experiments are needed to ascertain whether the two bands are associated with multiquasiparticle excitations coexisting with the wobbling excitation in the triaxial potential well.

ACKNOWLEDGMENTS

This material was based upon work supported by the US Department of Energy, Office of Science, Office of Nuclear Physics, under Grant No. DE-FG02-95ER40939 (MSU) and under Contract No. DE-AC03-76SF00098 (LBNL), by the Danish Science Foundation, and by the German BMBF under Grants No. 06 BN 907 and No. 06 BN 109. D.G.R. and W.C.M. thank Niels Bohr Institute for partial support during their visits. D.G.R acknowledges partial financial assistance provided by Rhodes University.

APPENDIX

The γ-ray energies, intensities, level energies, spin and parity assignments, as well as DCO ratios for new transitions, are listed in Table IV.

TABLE IV. γ-ray energies E_γ (in keV), suggested spins and parities of the initial (I_i^π) and final (I_f^π) states, excitation energies E_i (in keV) of initial states, DCO ratios, intensities (I_γ), and for interband linking transitions the band number (N) of the final states in ^{167}Lu.

E_γ[a]	$I_i^\pi \rightarrow I_f^\pi$[b]	E_i	DCO[c]	I_γ[d]	N
	Band 1				
140.0	$\frac{9}{2}^+ \rightarrow \frac{7}{2}^+$	140.0		147(29)	
305.3	$\frac{11}{2}^+ \rightarrow \frac{7}{2}^+$	305.3		443(33)	
165.3	$\frac{11}{2}^+ \rightarrow \frac{9}{2}^+$			375(36)	
354.1	$\frac{13}{2}^+ \rightarrow \frac{9}{2}^+$	494.2		660(60)	
188.9	$\frac{13}{2}^+ \rightarrow \frac{11}{2}^+$			253(28)	
399.0	$\frac{15}{2}^+ \rightarrow \frac{11}{2}^+$	704.3		828(66)	
210.3	$\frac{15}{2}^+ \rightarrow \frac{13}{2}^+$			240(22)	
439.7	$\frac{17}{2}^+ \rightarrow \frac{13}{2}^+$	934.1		960(120)	
230.0	$\frac{17}{2}^+ \rightarrow \frac{15}{2}^+$			216(31)	
477.0	$\frac{19}{2}^+ \rightarrow \frac{15}{2}^+$	1181.2		701(52)	
246.6	$\frac{19}{2}^+ \rightarrow \frac{17}{2}^+$			$\leqslant$216	
510.2	$\frac{21}{2}^+ \rightarrow \frac{17}{2}^+$	1444.4		894(66)	
263.6	$\frac{21}{2}^+ \rightarrow \frac{19}{2}^+$			128(10)	
539.0	$\frac{23}{2}^+ \rightarrow \frac{19}{2}^+$	1720.1		637(47)	

TABLE IV. (*Continued.*)

E_γ[a]	$I_i^\pi \rightarrow I_f^\pi$[b]	E_i	DCO[c]	I_γ[d]	N
275.8	$\frac{23}{2}^+ \rightarrow \frac{21}{2}^+$			100(9)	
563.6	$\frac{25}{2}^+ \rightarrow \frac{21}{2}^+$	2008.0		648(60)	
288.3	$\frac{25}{2}^+ \rightarrow \frac{23}{2}^+$			110(9)	
579.2	$\frac{27}{2}^+ \rightarrow \frac{23}{2}^+$	2299.3		525(40)	
291.2	$\frac{27}{2}^+ \rightarrow \frac{25}{2}^+$			68(7)	
572.6	$\frac{29}{2}^+ \rightarrow \frac{25}{2}^+$	2580.6		401(31)	
281.0	$\frac{29}{2}^+ \rightarrow \frac{27}{2}^+$			76(12)	
523.8	$\frac{31}{2}^+ \rightarrow \frac{27}{2}^+$	2823.1		268(21)	
242.1	$\frac{31}{2}^+ \rightarrow \frac{29}{2}^+$			81(8)	
463.0	$\frac{33}{2}^+ \rightarrow \frac{29}{2}^+$	3043.9		356(50)	
221.1	$\frac{33}{2}^+ \rightarrow \frac{31}{2}^+$			110(9)	
462.3	$\frac{35}{2}^+ \rightarrow \frac{31}{2}^+$	3285.4		185(38)	
241.2	$\frac{35}{2}^+ \rightarrow \frac{33}{2}^+$			109(12)	
488.4	$\frac{37}{2}^+ \rightarrow \frac{33}{2}^+$	3532.3		231(18)	
246.6	$\frac{37}{2}^+ \rightarrow \frac{35}{2}^+$			$\leqslant$138	
527.5	$\frac{39}{2}^+ \rightarrow \frac{35}{2}^+$	3812.9		211(17)	
280.7	$\frac{39}{2}^+ \rightarrow \frac{37}{2}^+$			48(9)	
563.9	$\frac{41}{2}^+ \rightarrow \frac{37}{2}^+$	4096.2		221(36)	
283.6	$\frac{41}{2}^+ \rightarrow \frac{39}{2}^+$			52(6)	
604.4	$\frac{43}{2}^+ \rightarrow \frac{39}{2}^+$	4417.4	0.99(2)	224(20)	
321.0	$\frac{43}{2}^+ \rightarrow \frac{41}{2}^+$		0.73(4)	$\leqslant$30	
639.1	$\frac{45}{2}^+ \rightarrow \frac{41}{2}^+$	4735.3	0.98(2)	261(22)	
317.7	$\frac{45}{2}^+ \rightarrow \frac{43}{2}^+$		0.68(4)	$\leqslant$48	
676.0	$\frac{47}{2}^+ \rightarrow \frac{43}{2}^+$	5093.3	1.00(4)	171(15)	
358.1	$\frac{47}{2}^+ \rightarrow \frac{45}{2}^+$		0.85(6)	$\leqslant$24	
707.6	$\frac{49}{2}^+ \rightarrow \frac{45}{2}^+$	5442.9	1.01(4)	214(19)	
349.6	$\frac{49}{2}^+ \rightarrow \frac{47}{2}^+$		0.72(11)	47(5)	
740.3	$\frac{51}{2}^+ \rightarrow \frac{47}{2}^+$	5833.4	0.97(4)	147(17)	
390.7	$\frac{51}{2}^+ \rightarrow \frac{49}{2}^+$		0.71(11)	28(4)	
770.0	$\frac{53}{2}^+ \rightarrow \frac{49}{2}^+$	6213.1	0.99(4)	161(15)	
379.5	$\frac{53}{2}^+ \rightarrow \frac{51}{2}^+$		0.76(15)	19(5)	
798.3	$\frac{55}{2}^+ \rightarrow \frac{51}{2}^+$	6631.6	0.99(4)	101(11)	
418.2	$\frac{55}{2}^+ \rightarrow \frac{53}{2}^+$		0.77(15)	17(2)	
823.4	$\frac{57}{2}^+ \rightarrow \frac{53}{2}^+$	7036.2	0.94(4)	112(40)	
404.8	$\frac{57}{2}^+ \rightarrow \frac{55}{2}^+$		0.67(10)	34(13)	
840.0	$\frac{59}{2}^+ \rightarrow \frac{55}{2}^+$	7471.4	0.98(10)	61(8)	
744.6	$\frac{59}{2}^+ \rightarrow \frac{55}{2}^+$			5(1)	10
434.7	$\frac{59}{2}^+ \rightarrow \frac{57}{2}^+$		0.66(13)	9(2)	
841.0	$\frac{61}{2}^+ \rightarrow \frac{57}{2}^+$	7877.2	0.97(5)	85(30)	
776.2	$\frac{61}{2}^+ \rightarrow \frac{57}{2}^+$			26(10)	10
871.3	$\frac{63}{2}^+ \rightarrow \frac{59}{2}^+$	8342.7	1.08(16)	37(4)	
871.9	$\frac{65}{2}^+ \rightarrow \frac{61}{2}^+$	8749.0	0.96(10)	64(23)	
927.5	$\frac{67}{2}^+ \rightarrow \frac{63}{2}^+$	9270.2	0.96(14)	28(3)	
925.1	$\frac{69}{2}^+ \rightarrow \frac{65}{2}^+$	9674.2	1.01(10)	55(20)	
993.7	$\frac{71}{2}^+ \rightarrow \frac{67}{2}^+$	10263.9	0.91(18)	10(2)	
980.3	$\frac{73}{2}^+ \rightarrow \frac{69}{2}^+$	10654.5	1.02(15)	30(11)	
1058.3	$\frac{75}{2}^+ \rightarrow \frac{71}{2}^+$	11322.2	1.13(23)	8(2)	
1036.1	$\frac{77}{2}^+ \rightarrow \frac{73}{2}^+$	11690.5	1.01(20)	19(7)	
1118.4	$\frac{79}{2}^+ \rightarrow \frac{75}{2}^+$	12440.6	0.90(18)	4(1)	
1090.4	$\frac{81}{2}^+ \rightarrow \frac{77}{2}^+$	12780.3	0.92(18)	7(3)	
1170.6	$\frac{83}{2}^+ \rightarrow \frac{79}{2}^+$	13609.8	1.07(21)	$\leqslant$3	
1140.8	$\frac{85}{2}^+ \rightarrow \frac{81}{2}^+$	13922.1	0.98(20)	$\leqslant$3	
1212.3	$\frac{87}{2}^+ \rightarrow \frac{83}{2}^+$	14822.1	1.04(21)	$\leqslant$3	
1186.4	$\frac{89}{2}^+ \rightarrow \frac{85}{2}^+$	15108.8	0.98(20)	$\leqslant$3	
1244.0	$(\frac{91}{2}^+) \rightarrow \frac{87}{2}^+$	16065.1		$\leqslant$3	
1231.2	$\frac{93}{2}^+ \rightarrow \frac{89}{2}^+$	16340.1	1.00(20)	$\leqslant$3	
1256.1	$(\frac{95}{2}^+) \rightarrow (\frac{91}{2}^+)$	17321.2		$\leqslant$3	
1278.6	$(\frac{97}{2}^+) \rightarrow \frac{93}{2}^+$	17617.8		$\leqslant$3	
	Band 2				
855.0	$\frac{19}{2}^- \rightarrow \frac{17}{2}^+$	1789.1		21(5)	1
263.5	$\frac{21}{2}^- \rightarrow (\frac{17}{2}^-)$	1940.6		95(11)	
781.0	$\frac{21}{2}^- \rightarrow \frac{19}{2}^-$			40(4)	15
759.4	$\frac{21}{2}^- \rightarrow \frac{19}{2}^+$			38(3)	1
311.2	$\frac{23}{2}^- \rightarrow \frac{19}{2}^-$	2100.3		38(2)	
159.7	$\frac{23}{2}^- \rightarrow \frac{21}{2}^-$			15(1)	
655.9	$\frac{23}{2}^- \rightarrow \frac{21}{2}^+$		0.65(3)	144(7)	1
345.0	$\frac{25}{2}^- \rightarrow \frac{21}{2}^-$	2285.6		77(7)	
185.3	$\frac{25}{2}^- \rightarrow \frac{23}{2}^-$		0.91(13)	42(4)	
565.4	$\frac{25}{2}^- \rightarrow \frac{23}{2}^+$		0.68(7)	66(6)	1
390.7	$\frac{27}{2}^- \rightarrow \frac{23}{2}^-$	2491.0	0.97(4)	105(8)	
205.4	$\frac{27}{2}^- \rightarrow \frac{25}{2}^-$		0.86(12)	38(3)	
483.0	$\frac{27}{2}^- \rightarrow \frac{25}{2}^+$		0.69(10)	22(2)	1
430.1	$\frac{29}{2}^- \rightarrow \frac{25}{2}^-$	2715.7	0.94(9)	56(6)	
224.7	$\frac{29}{2}^- \rightarrow \frac{27}{2}^-$		0.99(20)	13(2)	
467.8	$\frac{31}{2}^- \rightarrow \frac{27}{2}^-$	2958.8	0.97(10)	70(11)	
243.1	$\frac{31}{2}^- \rightarrow \frac{29}{2}^-$		1.07(21)	11(2)	
501.6	$\frac{33}{2}^- \rightarrow \frac{29}{2}^-$	3217.3	1.02(10)	55(11)	
258.5	$\frac{33}{2}^- \rightarrow \frac{31}{2}^-$		1.21(24)	7(2)	
532.8	$\frac{35}{2}^- \rightarrow \frac{31}{2}^-$	3491.6	1.00(10)	58(17)	
274.3	$\frac{35}{2}^- \rightarrow \frac{33}{2}^-$		0.99(20)	8(4)	
561.3	$\frac{37}{2}^- \rightarrow \frac{33}{2}^-$	3778.5	0.91(14)	40(14)	
287.0	$\frac{37}{2}^- \rightarrow \frac{35}{2}^-$		1.00(20)	6(2)	
586.4	$\frac{39}{2}^- \rightarrow \frac{35}{2}^-$	4078.0	0.99(10)	57(21)	
299.4	$\frac{39}{2}^- \rightarrow \frac{37}{2}^-$		1.02(20)	9(2)	

TABLE IV. (*Continued.*)

E_γ[a]	$I_i^\pi \rightarrow I_f^\pi$[b]	E_i	DCO[c]	I_γ[d]	N
607.3	$\frac{41}{2}^- \rightarrow \frac{37}{2}^-$	4385.8	0.95(10)	53(21)	
772.0	$\frac{41}{2}^- \rightarrow \frac{37}{2}^-$			⩽3	13
307.9	$\frac{41}{2}^- \rightarrow \frac{39}{2}^-$		0.91(18)	7(2)	
626.6	$\frac{43}{2}^- \rightarrow \frac{39}{2}^-$	4704.6	1.02(15)	44(17)	
318.8	$\frac{43}{2}^- \rightarrow \frac{41}{2}^-$		1.09(22)	5(1)	
644.7	$\frac{45}{2}^- \rightarrow \frac{41}{2}^-$	5030.8	0.98(15)	38(15)	
657.0	$\frac{45}{2}^- \rightarrow \frac{41}{2}^-$			9(4)	13
326.2	$\frac{45}{2}^- \rightarrow \frac{43}{2}^-$		0.81(16)	⩽3	
664.6	$\frac{47}{2}^- \rightarrow \frac{43}{2}^-$	5369.2	1.00(15)	41(17)	
338.4	$\frac{47}{2}^- \rightarrow \frac{45}{2}^-$		0.86(17)	7(6)	
684.0	$\frac{49}{2}^- \rightarrow \frac{45}{2}^-$	5714.8	1.05(16)	32(16)	
345.0	$\frac{49}{2}^- \rightarrow \frac{47}{2}^-$			10(9)	
707.9	$\frac{51}{2}^- \rightarrow \frac{47}{2}^-$	6077.1	0.96(14)	32(14)	
362.8	$\frac{51}{2}^- \rightarrow \frac{49}{2}^-$			9(4)	
733.1	$\frac{53}{2}^- \rightarrow \frac{49}{2}^-$	6448.1	1.08(16)	23(9)	
370.0	$\frac{53}{2}^- \rightarrow \frac{51}{2}^-$			4(2)	
761.6	$\frac{55}{2}^- \rightarrow \frac{51}{2}^-$	6838.7	0.94(14)	25(11)	
392.0	$\frac{55}{2}^- \rightarrow \frac{53}{2}^-$			7(3)	
792.1	$\frac{57}{2}^- \rightarrow \frac{53}{2}^-$	7240.2	0.93(19)	17(7)	
400.7	$\frac{57}{2}^- \rightarrow \frac{55}{2}^-$			5(2)	
823.3	$\frac{59}{2}^- \rightarrow \frac{55}{2}^-$	7662.0	0.93(19)	17(8)	
423.0	$\frac{59}{2}^- \rightarrow \frac{57}{2}^-$			⩽3	
855.9	$\frac{61}{2}^- \rightarrow \frac{57}{2}^-$	8096.0	0.96(19)	13(5)	
886.9	$\frac{63}{2}^- \rightarrow \frac{59}{2}^-$	8548.9	0.96(19)	13(5)	
919.5	$\frac{65}{2}^- \rightarrow \frac{61}{2}^-$	9015.5	1.03(21)	8(4)	
948.7	$\frac{67}{2}^- \rightarrow \frac{63}{2}^-$	9497.6	1.02(20)	8(4)	
981.1	$\frac{69}{2}^- \rightarrow \frac{65}{2}^-$	9996.8	0.95(19)	⩽3	
982.5	$\frac{69}{2}^- \rightarrow \frac{65}{2}^-$			⩽3	14
1005.9	$\frac{71}{2}^- \rightarrow \frac{67}{2}^-$	10503.5	0.94(19)	5(2)	
1039.5	$\frac{73}{2}^- \rightarrow \frac{69}{2}^-$	11036.5	0.90(18)	⩽3	
1054.8	$\frac{75}{2}^- \rightarrow \frac{71}{2}^-$	11558.3	0.97(19)	4(2)	
1102.0	$\frac{77}{2}^- \rightarrow \frac{73}{2}^-$	12138.5	0.98(20)	⩽3	
1112.3	$\frac{77}{2}^- \rightarrow \frac{73}{2}^-$			⩽3	14
1098.1	$\frac{79}{2}^- \rightarrow \frac{75}{2}^-$	12656.4	0.98(20)	4(2)	
(1151.8)	$(\frac{81}{2}^-) \rightarrow \frac{77}{2}^-$	13290.3		⩽3	
1138.4	$(\frac{83}{2}^-) \rightarrow \frac{79}{2}^-$	13794.9		⩽3	
1169.6	$(\frac{87}{2}^-) \rightarrow (\frac{83}{2}^-)$	14964.4		⩽3	
	Band 3				
658.7	$\frac{25}{2}^- \rightarrow \frac{23}{2}^+$	2379.1	0.69(7)	50(5)	1
504.9	$\frac{29}{2}^- \rightarrow \frac{25}{2}^-$	2884.2	0.95(19)	52(9)	
534.4	$\frac{33}{2}^- \rightarrow \frac{29}{2}^-$	3418.6	1.18(15)	57(10)	

TABLE IV. (*Continued.*)

E_γ[a]	$I_i^\pi \rightarrow I_f^\pi$[b]	E_i	DCO[c]	I_γ[d]	N
260.0	$\frac{35}{2}^- \rightarrow \frac{33}{2}^-$	3678.9		5(2)	
530.6	$\frac{37}{2}^- \rightarrow \frac{33}{2}^-$	3949.2	0.98(10)	51(10)	
270.4	$\frac{37}{2}^- \rightarrow \frac{35}{2}^-$		0.61(6)	22(6)	
566.3	$\frac{39}{2}^- \rightarrow \frac{35}{2}^-$	4245.2		23(6)	
295.7	$\frac{39}{2}^- \rightarrow \frac{37}{2}^-$			4(1)	
596.0	$\frac{41}{2}^- \rightarrow \frac{37}{2}^-$	4545.2		32(8)	
300.3	$\frac{41}{2}^- \rightarrow \frac{39}{2}^-$			4(1)	
636.2	$\frac{43}{2}^- \rightarrow \frac{39}{2}^-$	4881.4		29(8)	
335.9	$\frac{43}{2}^- \rightarrow \frac{41}{2}^-$			9(3)	
640.0	$\frac{45}{2}^- \rightarrow \frac{41}{2}^-$	5185.2	1.13(17)	33(9)	
304.1	$\frac{45}{2}^- \rightarrow \frac{43}{2}^-$			5(2)	
659.3	$\frac{47}{2}^- \rightarrow \frac{43}{2}^-$	5540.7		28(7)	
355.5	$\frac{47}{2}^- \rightarrow \frac{45}{2}^-$			7(2)	
674.9	$\frac{49}{2}^- \rightarrow \frac{45}{2}^-$	5860.1	0.97(4)	38(10)	
319.4	$\frac{49}{2}^- \rightarrow \frac{47}{2}^-$			⩽3	
702.1	$\frac{51}{2}^- \rightarrow \frac{47}{2}^-$	6242.8		30(8)	
382.5	$\frac{51}{2}^- \rightarrow \frac{49}{2}^-$			⩽3	
733.0	$\frac{53}{2}^- \rightarrow \frac{49}{2}^-$	6593.1	0.97(4)	37(9)	
350.1	$\frac{53}{2}^- \rightarrow \frac{51}{2}^-$			⩽3	
759.0	$\frac{55}{2}^- \rightarrow \frac{51}{2}^-$	7001.8	0.97(4)	32(8)	
408.7	$\frac{55}{2}^- \rightarrow \frac{53}{2}^-$			⩽3	
791.0	$\frac{57}{2}^- \rightarrow \frac{53}{2}^-$	7384.1	1.02(4)	36(9)	
823.0	$\frac{59}{2}^- \rightarrow \frac{55}{2}^-$	7824.8	1.02(4)	32(8)	
843.8	$\frac{61}{2}^- \rightarrow \frac{57}{2}^-$	8227.9	0.93(6)	37(9)	
887.0	$\frac{63}{2}^- \rightarrow \frac{59}{2}^-$	8711.8	0.93(6)	33(8)	
893.1	$(\frac{65}{2}^-) \rightarrow \frac{61}{2}^-$	9121.0		26(7)	
946.0	$(\frac{67}{2}^-) \rightarrow \frac{63}{2}^-$	9657.8		29(7)	
950.4	$(\frac{69}{2}^-) \rightarrow (\frac{65}{2}^-)$	10071.5		28(8)	
998.0	$(\frac{71}{2}^-) \rightarrow (\frac{67}{2}^-)$	10655.8		20(5)	
1013.2	$(\frac{73}{2}^-) \rightarrow (\frac{69}{2}^-)$	11084.7		22(6)	
1070.6	$(\frac{77}{2}^-) \rightarrow (\frac{73}{2}^-)$	12155.2		11(3)	
1136.1	$(\frac{81}{2}^-) \rightarrow (\frac{77}{2}^-)$	13291.3		7(2)	
	Band 4				
853.0	$\frac{25}{2}^+ \rightarrow \frac{23}{2}^-$	2508.9	0.63(13)	13(1)	15
993.7	$\frac{27}{2}^+ \rightarrow \frac{25}{2}^-$	2697.2		12(2)	13
962.0	$\frac{27}{2}^+ \rightarrow \frac{25}{2}^-$	2665.5	0.53(11)	13(4)	13
808.5	$\frac{27}{2}^+ \rightarrow \frac{23}{2}^+$			10(2)	8
384.3	$\frac{29}{2}^+ \rightarrow \frac{25}{2}^+$	2893.2	0.91(18)	11(1)	
632.2	$\frac{29}{2}^+ \rightarrow \frac{25}{2}^+$			4(1)	8
705.8	$\frac{29}{2}^+ \rightarrow \frac{25}{2}^+$			4(1)	9
424.0	$\frac{31}{2}^+ \rightarrow \frac{27}{2}^+$	3121.3		5(1)	
455.8	$\frac{31}{2}^+ \rightarrow \frac{27}{2}^+$		1.06(21)	28(8)	

TABLE IV. (*Continued.*)

E_γ [a]	$I_i^\pi \rightarrow I_f^\pi$ [b]	E_i	DCO[c]	I_γ [d]	N
723.1	$\frac{31}{2}^+ \rightarrow \frac{27}{2}^+$			$\leqslant 3$	8
843.1	$\frac{31}{2}^+ \rightarrow \frac{29}{2}^-$		0.50(10)	7(1)	13
464.1	$\frac{33}{2}^+ \rightarrow \frac{29}{2}^+$	3356.8	1.00(20)	8(1)	
235.4	$\frac{33}{2}^+ \rightarrow \frac{29}{2}^+$			$\leqslant 3$	
504.6	$\frac{35}{2}^+ \rightarrow \frac{31}{2}^+$	3625.9	1.08(16)	35(4)	
269.1	$\frac{35}{2}^+ \rightarrow \frac{33}{2}^+$			4(1)	
535.3	$\frac{37}{2}^+ \rightarrow \frac{33}{2}^+$	3892.1	0.98(20)	8(1)	
266.6	$\frac{37}{2}^+ \rightarrow \frac{35}{2}^+$			$\leqslant 3$	
567.4	$\frac{39}{2}^+ \rightarrow \frac{35}{2}^+$	4193.2	0.99(15)	28(2)	
300.0	$\frac{39}{2}^+ \rightarrow \frac{37}{2}^+$			5(1)	
603.6	$\frac{39}{2}^+ \rightarrow \frac{35}{2}^+$			6(1)	6
603.5	$\frac{41}{2}^+ \rightarrow \frac{37}{2}^+$	4496.0	0.99(20)	10(2)	
622.4	$\frac{43}{2}^- \rightarrow \frac{39}{2}^+$	4815.7	0.94(14)	26(2)	
319.7	$\frac{43}{2}^+ \rightarrow \frac{41}{2}^+$			$\leqslant 3$	
664.4	$\frac{45}{2}^+ \rightarrow \frac{41}{2}^+$	5160.3	1.04(21)	6(1)	
670.9	$\frac{47}{2}^+ \rightarrow \frac{43}{2}^+$	5486.6	0.94(14)	24(2)	
713.6	$\frac{49}{2}^+ \rightarrow \frac{45}{2}^+$	5873.9	1.02(20)	7(1)	
716.1	$\frac{51}{2}^+ \rightarrow \frac{47}{2}^+$	6202.7	0.99(15)	22(2)	
754.4	$\frac{53}{2}^+ \rightarrow \frac{49}{2}^+$	6628.4	1.00(20)	3(1)	
763.2	$\frac{55}{2}^+ \rightarrow \frac{51}{2}^+$	6965.9	0.94(19)	14(2)	
821.4	$\frac{57}{2}^+ \rightarrow \frac{53}{2}^+$	7450.3	1.00(20)	4(1)	
788.0	$\frac{57}{2}^+ \rightarrow \frac{53}{2}^+$			$\leqslant 3$	5
810.0	$\frac{59}{2}^+ \rightarrow \frac{55}{2}^+$	7775.9	1.01(19)	12(2)	
849.4	$(\frac{61}{2}^+) \rightarrow \frac{57}{2}^+$	8299.2		$\leqslant 3$	
871.0	$\frac{63}{2}^+ \rightarrow \frac{59}{2}^+$	8646.9	0.99(20)	6(2)	
911.3	$(\frac{65}{2}^+) \rightarrow (\frac{61}{2}^+)$	9210.5		$\leqslant 3$	
924.7	$\frac{67}{2}^+ \rightarrow \frac{63}{2}^+$	9571.6	1.04(21)	4(2)	
982.5	$(\frac{69}{2}^+) \rightarrow (\frac{65}{2}^+)$	10193.0		$\leqslant 3$	
979.9	$\frac{71}{2}^+ \rightarrow \frac{67}{2}^+$	10551.5	0.98(20)	$\leqslant 3$	
1026.4	$(\frac{73}{2}^+) \rightarrow (\frac{69}{2}^+)$	11219.4		$\leqslant 3$	
1036.6	$\frac{75}{2}^+ \rightarrow \frac{71}{2}^+$	11588.1	1.11(22)	$\leqslant 3$	
1099.0	$(\frac{79}{2}^+) \rightarrow \frac{75}{2}^+$	12687.5		$\leqslant 3$	
1164.1	$(\frac{83}{2}^+) \rightarrow (\frac{79}{2}^+)$	13851.5		$\leqslant 3$	
	Band 5				
788.0	$\frac{53}{2}^+ \rightarrow \frac{49}{2}^+$	6662.3		$\leqslant 3$	4
(741.0)	$\frac{57}{2}^+ \rightarrow \frac{53}{2}^+$	7403.3		$\leqslant 3$	
774.9	$\frac{57}{2}^+ \rightarrow \frac{53}{2}^+$		0.99(20)	$\leqslant 3$	4
826.0	$\frac{61}{2}^+ \rightarrow \frac{57}{2}^+$	8229.2		$\leqslant 3$	
	Band 6				
736.4	$\frac{31}{2}^+ \rightarrow \frac{29}{2}^-$	3014.8	0.67(13)	10(2)	13
616.6	$\frac{31}{2}^+ \rightarrow \frac{27}{2}^+$			32(8)	8
574.8	$\frac{35}{2}^+ \rightarrow \frac{31}{2}^+$	3589.6		15(2)	

TABLE IV. (*Continued.*)

E_γ [a]	$I_i^\pi \rightarrow I_f^\pi$ [b]	E_i	DCO[c]	I_γ [d]	N
670.8	$\frac{35}{2}^+ \rightarrow \frac{33}{2}^-$		0.64(6)	52(12)	13
650.4	$\frac{35}{2}^+ \rightarrow \frac{31}{2}^+$			23(6)	8
633.2	$\frac{39}{2}^+ \rightarrow \frac{35}{2}^+$	4222.8	0.97(4)	64(16)	
597.0	$\frac{39}{2}^+ \rightarrow \frac{35}{2}^+$			11(3)	4
609.4	$\frac{39}{2}^+ \rightarrow \frac{37}{2}^-$		0.64(5)	10(3)	13
675.5	$\frac{43}{2}^+ \rightarrow \frac{39}{2}^+$	4898.3	1.10(7)	74(19)	
524.9	$\frac{43}{2}^+ \rightarrow \frac{41}{2}^-$		0.69(6)	8(2)	13
726.7	$\frac{47}{2}^+ \rightarrow \frac{43}{2}^+$	5625.0	0.95(10)	70(18)	
780.6	$\frac{51}{2}^+ \rightarrow \frac{47}{2}^+$	6405.3	0.86(13)	67(17)	
829.3	$\frac{55}{2}^+ \rightarrow \frac{51}{2}^+$	7234.6	0.90(14)	46(12)	
864.4	$(\frac{59}{2}^+) \rightarrow \frac{55}{2}^+$	8099.0		42(11)	
904.2	$(\frac{63}{2}^+) \rightarrow (\frac{59}{2}^+)$	9003.2		19(5)	
	Band 7				
720.2	$\frac{29}{2}^+ \rightarrow \frac{25}{2}^+$	2728.3	0.94(9)	63(13)	1
593.9	$\frac{33}{2}^+ \rightarrow \frac{29}{2}^+$	3322.3	0.99(11)	23(5)	
741.8	$\frac{33}{2}^+ \rightarrow \frac{29}{2}^+$		0.96(5)	29(6)	1
650.1	$\frac{37}{2}^+ \rightarrow \frac{33}{2}^+$	3972.4	0.94(7)	31(6)	
622.4	$\frac{41}{2}^+ \rightarrow \frac{37}{2}^+$	4594.9	1.02(10)	16(3)	
636.0	$\frac{45}{2}^+ \rightarrow \frac{41}{2}^+$	5230.9	1.07(6)	12(2)	
664.1	$\frac{49}{2}^+ \rightarrow \frac{45}{2}^+$	5894.9	0.98(5)	7(1)	
705.0	$\frac{53}{2}^+ \rightarrow \frac{49}{2}^+$	6600.0	0.97(5)	$\leqslant 3$	
725.8	$\frac{53}{2}^+ \rightarrow \frac{49}{2}^+$			$\leqslant 3$	4
775.1	$\frac{57}{2}^+ \rightarrow \frac{53}{2}^+$	7374.9	0.96(10)	$\leqslant 3$	
	Band 8				
144.6	$\frac{5}{2}^+ \rightarrow \frac{1}{2}^+$	178.5			
129.7	$\frac{5}{2}^+ \rightarrow \frac{3}{2}^+$				
169.8	$\frac{7}{2}^+ \rightarrow \frac{3}{2}^+$	218.6	1.00(4)		
254.5	$\frac{9}{2}^+ \rightarrow \frac{5}{2}^+$	433.0	0.99(10)	56(6)	
214.5	$\frac{9}{2}^+ \rightarrow \frac{7}{2}^+$		0.81(8)	57(6)	
248.3	$\frac{9}{2}^+ \rightarrow \frac{7}{2}^+$		0.84(13)	20(3)	9
289.4	$\frac{11}{2}^+ \rightarrow \frac{7}{2}^+$	508.0	0.97(4)	175(17)	
178.2	$\frac{11}{2}^+ \rightarrow \frac{9}{2}^+$		0.82(4)	95(10)	9
351.0	$\frac{13}{2}^+ \rightarrow \frac{9}{2}^+$	784.0	0.94(4)	126(13)	
276.0	$\frac{13}{2}^+ \rightarrow \frac{11}{2}^+$		0.67(13)	14(2)	
284.5	$\frac{13}{2}^+ \rightarrow \frac{11}{2}^+$		0.65(10)	40(5)	9
379.2	$\frac{15}{2}^+ \rightarrow \frac{11}{2}^+$	887.5	0.96(4)	173(17)	
388.3	$\frac{15}{2}^+ \rightarrow \frac{11}{2}^+$		0.96(4)	164(40)	9
193.5	$\frac{15}{2}^+ \rightarrow \frac{13}{2}^+$		0.69(14)	9(1)	9
406.5	$\frac{15}{2}^+ \rightarrow \frac{13}{2}^-$			$\leqslant 3$	13
433.3	$\frac{17}{2}^+ \rightarrow \frac{13}{2}^+$	1217.3	1.05(4)	$\sim$169(20)[e]	
329.8	$\frac{17}{2}^+ \rightarrow \frac{15}{2}^+$		0.56(8)	44(5)	

TABLE IV. (*Continued.*)

E_γ[a]	$I_i^\pi \rightarrow I_f^\pi$[b]	E_i	DCO[c]	I_γ[d]	N
301.0	$\frac{17}{2}^+ \rightarrow \frac{15}{2}^+$		0.69(14)	11(2)	9
459.0	$\frac{19}{2}^+ \rightarrow \frac{15}{2}^+$	1347.0	1.03(4)	228(57)	
205.3	$\frac{19}{2}^+ \rightarrow \frac{17}{2}^+$		0.77(15)	5(1)	9
499.8	$\frac{21}{2}^+ \rightarrow \frac{17}{2}^+$	1717.1	1.11(3)	156(16)	
370.1	$\frac{21}{2}^+ \rightarrow \frac{19}{2}^+$		0.83(12)	21(2)	
310.0	$\frac{21}{2}^+ \rightarrow \frac{19}{2}^+$		0.84(4)	90(9)	9
510.0	$\frac{23}{2}^+ \rightarrow \frac{19}{2}^+$	1857.0	1.07(4)	210(40)	
651.5	$\frac{23}{2}^+ \rightarrow \frac{21}{2}^-$			17(4)	13
544.0	$\frac{25}{2}^+ \rightarrow \frac{21}{2}^+$	2261.0	0.92(4)	104(26)	
306.0	$\frac{25}{2}^+ \rightarrow \frac{23}{2}^+$		0.79(8)	60(7)	9
541.2	$\frac{27}{2}^+ \rightarrow \frac{23}{2}^+$	2398.2	1.10(4)[e]	∼140(27)[e]	
694.7	$\frac{27}{2}^+ \rightarrow \frac{25}{2}^-$			12(3)	13
516.0	$\frac{29}{2}^+ \rightarrow \frac{25}{2}^+$	2777.0		64(13)	
270.2	$\frac{29}{2}^+ \rightarrow \frac{27}{2}^+$			28(3)	9
541.2	$\frac{31}{2}^+ \rightarrow \frac{27}{2}^+$	2939.2	1.10(4)[e]	∼90(18)[e]	
162.2	$\frac{31}{2}^+ \rightarrow \frac{29}{2}^+$			⩽3	
660.9	$\frac{31}{2}^+ \rightarrow \frac{29}{2}^-$			9(3)	13
434.0	$\frac{33}{2}^+ \rightarrow \frac{29}{2}^+$	3211.1		∼54(13)[e]	
272.0	$\frac{33}{2}^+ \rightarrow \frac{31}{2}^+$			6(1)	
475.0	$\frac{35}{2}^+ \rightarrow \frac{31}{2}^+$	3414.1	1.02(10)	68(7)	
203.1	$\frac{35}{2}^+ \rightarrow \frac{33}{2}^+$			19(2)	
510.4	$\frac{37}{2}^+ \rightarrow \frac{33}{2}^+$	3721.5		57(14)	
307.4	$\frac{37}{2}^+ \rightarrow \frac{35}{2}^+$			19(2)	
544.0	$\frac{39}{2}^+ \rightarrow \frac{35}{2}^+$	3958.1	1.12(17)	38(4)	
586.4	$\frac{41}{2}^+ \rightarrow \frac{37}{2}^+$	4307.9		55(6)	
620.2	$\frac{43}{2}^+ \rightarrow \frac{39}{2}^+$	4578.3	1.05(16)	30(10)	
687.0	$\frac{47}{2}^+ \rightarrow \frac{43}{2}^+$	5265.3	1.07(16)	29(3)	
735.6	$\frac{51}{2}^+ \rightarrow \frac{47}{2}^+$	6015.8		7(1)	10
750.4	$\frac{51}{2}^+ \rightarrow \frac{47}{2}^+$		1.07(21)	18(2)	
804.7	$\frac{55}{2}^+ \rightarrow \frac{51}{2}^+$	6820.5	0.97(19)	20(2)	
864.7	$\frac{59}{2}^+ \rightarrow \frac{55}{2}^+$	7685.2	0.97(19)	14(2)	
915.2	$\frac{63}{2}^+ \rightarrow \frac{59}{2}^+$	8600.4	0.92(18)	12(2)	
942.1	$\frac{67}{2}^+ \rightarrow \frac{63}{2}^+$	9542.5	0.96(19)	⩽3	
989.3	$\frac{71}{2}^+ \rightarrow \frac{67}{2}^+$	10531.8	0.90(18)	⩽3	
1040.0	$(\frac{75}{2}^+) \rightarrow \frac{71}{2}^+$	11571.8		⩽3	
	Band 9				
117.4	$\frac{7}{2}^+ \rightarrow \frac{5}{2}^+$	184.7	0.85(4)		
262.4	$\frac{9}{2}^+ \rightarrow \frac{5}{2}^+$	329.7	0.90(14)	27(5)	
145.0	$\frac{9}{2}^+ \rightarrow \frac{7}{2}^+$		0.80(8)	195(33)	
314.5	$\frac{11}{2}^+ \rightarrow \frac{7}{2}^+$	499.2	0.93(18)	73(7)	
169.4	$\frac{11}{2}^+ \rightarrow \frac{9}{2}^+$		0.74(7)	141(11)	
364.6	$\frac{13}{2}^+ \rightarrow \frac{9}{2}^+$	694.0	1.01(4)	129(13)	

TABLE IV. (*Continued.*)

E_γ[a]	$I_i^\pi \rightarrow I_f^\pi$[b]	E_i	DCO[c]	I_γ[d]	N
194.8	$\frac{13}{2}^+ \rightarrow \frac{11}{2}^+$		0.82(9)	58(5)	
186.0	$\frac{13}{2}^+ \rightarrow \frac{11}{2}^+$		0.68(7)	79(8)	8
417.4	$\frac{15}{2}^+ \rightarrow \frac{11}{2}^+$	916.4	1.00(10)	60(5)	
222.4	$\frac{15}{2}^+ \rightarrow \frac{13}{2}^+$		0.81(5)	89(7)	
408.4	$\frac{15}{2}^+ \rightarrow \frac{11}{2}^+$		0.93(9)	71(7)	8
447.5	$\frac{17}{2}^+ \rightarrow \frac{13}{2}^+$	1141.6	0.91(4)	109(7)	
225.3	$\frac{17}{2}^+ \rightarrow \frac{15}{2}^+$		0.68(16)	68(3)	
254.0	$\frac{17}{2}^+ \rightarrow \frac{15}{2}^+$		0.81(16)	14(1)	8
490.4	$\frac{19}{2}^+ \rightarrow \frac{15}{2}^+$	1406.8	1.04(4)	127(5)	
265.2	$\frac{19}{2}^+ \rightarrow \frac{17}{2}^+$		0.77(12)	37(2)	
189.5	$\frac{19}{2}^+ \rightarrow \frac{17}{2}^+$		0.78(16)	15(1)	8
508.7	$\frac{21}{2}^+ \rightarrow \frac{17}{2}^+$	1650.2	0.93(4)[e]	∼110(22)[e]	
243.4	$\frac{21}{2}^+ \rightarrow \frac{19}{2}^+$		0.75(11)	39(3)	
548.0	$\frac{23}{2}^+ \rightarrow \frac{19}{2}^+$	1955.1	1.00(5)	102(7)	
304.9	$\frac{23}{2}^+ \rightarrow \frac{21}{2}^+$		0.73(11)	28(1)	
238.0	$\frac{23}{2}^+ \rightarrow \frac{21}{2}^+$		0.80(16)	8(1)	8
537.3	$\frac{25}{2}^+ \rightarrow \frac{21}{2}^+$	2187.4	0.98(4)	100(20)	
232.3	$\frac{25}{2}^+ \rightarrow \frac{23}{2}^+$		0.82(12)	24(3)	
551.7	$\frac{27}{2}^+ \rightarrow \frac{23}{2}^+$	2506.8	1.05(5)	72(14)	
319.4	$\frac{27}{2}^+ \rightarrow \frac{25}{2}^+$		0.52(10)	12(2)	
245.8	$\frac{27}{2}^+ \rightarrow \frac{25}{2}^+$		0.63(16)	29(3)	8
508.0	$\frac{29}{2}^+ \rightarrow \frac{25}{2}^+$	2695.1	0.93(4)[e]	∼105(21)[e]	
188.2	$\frac{29}{2}^+ \rightarrow \frac{27}{2}^+$		0.83(8)	51(4)	
452.3	$\frac{31}{2}^+ \rightarrow \frac{27}{2}^+$	2959.2	0.97(10)	57(4)	
264.1	$\frac{31}{2}^+ \rightarrow \frac{29}{2}^+$		0.83(8)	66(7)	
439.0	$\frac{33}{2}^+ \rightarrow \frac{29}{2}^+$	3134.1	1.03(4)	115(13)	
174.9	$\frac{33}{2}^+ \rightarrow \frac{31}{2}^+$		0.66(11)	21(2)	
478.4	$\frac{35}{2}^+ \rightarrow \frac{31}{2}^+$	3437.7	1.01(10)	58(5)	
303.6	$\frac{35}{2}^+ \rightarrow \frac{33}{2}^+$		0.67(13)	19(2)	
226.6	$\frac{35}{2}^+ \rightarrow \frac{33}{2}^+$			6(1)	8
478.9	$\frac{35}{2}^+ \rightarrow \frac{31}{2}^+$			23(5)	8
494.8	$\frac{37}{2}^+ \rightarrow \frac{33}{2}^+$	3628.9	1.02(4)	103(10)	
191.2	$\frac{37}{2}^+ \rightarrow \frac{35}{2}^+$		0.74(15)	11(2)	
214.6	$\frac{37}{2}^+ \rightarrow \frac{35}{2}^+$			12(2)	8
541.6	$\frac{39}{2}^+ \rightarrow \frac{35}{2}^+$	3979.3		44(9)	
350.4	$\frac{39}{2}^+ \rightarrow \frac{37}{2}^+$			16(3)	
561.1	$\frac{39}{2}^+ \rightarrow \frac{35}{2}^+$			20(4)	
577.3	$\frac{41}{2}^+ \rightarrow \frac{37}{2}^+$	4206.2	0.97(5)	95(10)	
226.9	$\frac{41}{2}^+ \rightarrow \frac{39}{2}^+$			3(1)	
618.6	$\frac{43}{2}^+ \rightarrow \frac{39}{2}^+$	4597.5	1.02(15)	21(8)	
391.3	$\frac{43}{2}^+ \rightarrow \frac{41}{2}^+$			7(2)	
655.3	$\frac{45}{2}^+ \rightarrow \frac{41}{2}^+$	4861.5	0.94(5)	90(9)	

TABLE IV. (*Continued.*)

E_γ[a]	$I_i^\pi \rightarrow I_f^\pi$[b]	E_i	DCO[c]	I_γ[d]	N
264.0	$\frac{45}{2}^+ \rightarrow \frac{43}{2}^+$			10(2)	
725.2	$\frac{49}{2}^+ \rightarrow \frac{45}{2}^+$	5586.7	1.04(10)	59(6)	
307.2	$\frac{49}{2}^+ \rightarrow \frac{47}{2}^+$			7(1)	10
801.8	$\frac{53}{2}^+ \rightarrow \frac{49}{2}^+$	6388.5	0.95(4)	34(3)	
757.6	$\frac{53}{2}^+ \rightarrow \frac{49}{2}^+$			11(1)	10
853.5	$\frac{57}{2}^+ \rightarrow \frac{53}{2}^+$	7242.0	1.02(15)	23(2)	
901.9	$\frac{61}{2}^+ \rightarrow \frac{57}{2}^+$	8144.0	1.05(21)	12(1)	
815.2	$\frac{61}{2}^+ \rightarrow \frac{57}{2}^+$		0.99(20)	$\leqslant$3	11
894.2	$\frac{65}{2}^+ \rightarrow \frac{61}{2}^+$	9038.2	1.09(22)	10(1)	
854.9	$\frac{65}{2}^+ \rightarrow \frac{61}{2}^+$		1.10(22)[e]	6(2)	11
931.8	$\frac{69}{2}^+ \rightarrow \frac{65}{2}^+$	9970.0	1.01(20)	15(2)	
988.0	$\frac{73}{2}^+ \rightarrow \frac{69}{2}^+$	10958.1	1.03(21)	10(1)	
1054.0	$\frac{77}{2}^+ \rightarrow \frac{73}{2}^+$	12012.0	1.11(22)	8(1)	
1120.1	$\frac{81}{2}^+ \rightarrow \frac{77}{2}^+$	13132.2	1.02(20)	6(1)	
1183.3	$\frac{85}{2}^+ \rightarrow \frac{81}{2}^+$	14315.4	0.97(19)	4(1)	
1243.2	$(\frac{89}{2}^+) \rightarrow \frac{85}{2}^+$	15558.5		$\leqslant$3	
	Band 10				
647.0	$\frac{45}{2}^+ \rightarrow \frac{41}{2}^+$	4954.9	1.02(15)	47(6)	8
682.0	$\frac{47}{2}^+ \rightarrow \frac{43}{2}^+$	5279.5	1.01(15)	29(3)	9
418.0	$\frac{47}{2}^+ \rightarrow \frac{45}{2}^+$			$\leqslant$3	9
676.0	$\frac{49}{2}^+ \rightarrow \frac{45}{2}^+$	5630.9	1.03(15)	47(6)	
702.8	$\frac{51}{2}^+ \rightarrow \frac{47}{2}^+$	5982.3	0.99(15)	20(2)	
351.4	$\frac{51}{2}^+ \rightarrow \frac{49}{2}^+$			32(7)	
395.6	$\frac{51}{2}^+ \rightarrow \frac{49}{2}^+$			4(1)	9
717.0	$\frac{51}{2}^+ \rightarrow \frac{47}{2}^+$			20(2)	8
702.0	$\frac{53}{2}^+ \rightarrow \frac{49}{2}^+$	6332.9	1.01(15)	47(6)	
890.0	$\frac{53}{2}^+ \rightarrow \frac{49}{2}^+$			15(2)	1
746.4	$\frac{53}{2}^+ \rightarrow \frac{49}{2}^+$			$\leqslant$3	9
350.6	$\frac{53}{2}^+ \rightarrow \frac{51}{2}^+$			9(2)	
744.4	$\frac{55}{2}^+ \rightarrow \frac{51}{2}^+$	6726.8	0.95(19)	15(2)	
393.9	$\frac{55}{2}^+ \rightarrow \frac{53}{2}^+$			6(2)	
768.1	$\frac{57}{2}^+ \rightarrow \frac{53}{2}^+$	7101.0	1.03(15)	48(6)	
374.2	$\frac{57}{2}^+ \rightarrow \frac{55}{2}^+$			7(2)	
888.4	$\frac{57}{2}^+ \rightarrow \frac{53}{2}^+$			18(7)	1
816.6	$\frac{59}{2}^+ \rightarrow \frac{55}{2}^+$	7543.4	1.09(22)	12(2)	
912.0	$\frac{59}{2}^+ \rightarrow \frac{55}{2}^+$			9(2)	1
866.9	$\frac{61}{2}^+ \rightarrow \frac{57}{2}^+$	7967.9	0.99(15)	39(5)	
931.7	$\frac{61}{2}^+ \rightarrow \frac{57}{2}^+$		0.93(14)	17(4)	1
912.6	$\frac{63}{2}^+ \rightarrow \frac{59}{2}^+$	8456.0	0.98(5)	10(1)	
957.0	$\frac{65}{2}^+ \rightarrow \frac{61}{2}^+$	8924.9	0.95(14)	28(8)	
987.1	$\frac{67}{2}^+ \rightarrow \frac{63}{2}^+$	9443.1	1.22(24)	9(1)	

TABLE IV. (*Continued.*)

E_γ[a]	$I_i^\pi \rightarrow I_f^\pi$[b]	E_i	DCO[c]	I_γ[d]	N
1022.0	$\frac{69}{2}^+ \rightarrow \frac{65}{2}^+$	9946.9	0.91(18)	27(8)	
1046.2	$\frac{71}{2}^+ \rightarrow \frac{67}{2}^+$	10489.1	0.87(17)	8(1)	
1084.1	$(\frac{73}{2}^+) \rightarrow \frac{69}{2}^+$	11031.0		14(3)	
1105.3	$\frac{75}{2}^+ \rightarrow \frac{71}{2}^+$	11594.1	1.08(22)	6(1)	
1137.1	$(\frac{77}{2}^+) \rightarrow (\frac{73}{2}^+)$	12167.9		9(2)	
	Band 11				
562.0	$\frac{25}{2}^+ \rightarrow \frac{21}{2}^+$	2278.7	1.02(4)[e]	$\leqslant$3	8
399.3	$\frac{29}{2}^+ \rightarrow (\frac{25}{2}^+)$	2749.7		17(3)	
562.3	$\frac{29}{2}^+ \rightarrow \frac{25}{2}^+$		1.02(4)[e]	20(3)	9
471.0	$\frac{29}{2}^+ \rightarrow \frac{25}{2}^+$			$\leqslant$3	
242.9	$\frac{29}{2}^+ \rightarrow \frac{27}{2}^+$		0.82(12)	9(3)	9
351.0	$\frac{29}{2}^+ \rightarrow \frac{27}{2}^+$		0.85(13)	10(3)	8
488.6	$\frac{29}{2}^+ \rightarrow \frac{25}{2}^+$		0.95(10)	22(4)	8
504.7	$\frac{33}{2}^+ \rightarrow \frac{29}{2}^+$	3254.6	0.90(5)	78(9)	
559.8	$\frac{33}{2}^+ \rightarrow \frac{29}{2}^+$		1.02(4)[e]	55(8)	9
560.6	$\frac{37}{2}^+ \rightarrow \frac{33}{2}^+$	3815.3	1.02(4)[e]	90(9)	
606.8	$\frac{41}{2}^+ \rightarrow \frac{37}{2}^+$	4422.1	1.07(11)	78(7)	
654.6	$\frac{45}{2}^+ \rightarrow \frac{41}{2}^+$	5076.7	0.91(4)	64(6)	
701.8	$\frac{49}{2}^+ \rightarrow \frac{45}{2}^+$	5778.5	1.00(10)	49(5)	
751.6	$\frac{53}{2}^+ \rightarrow \frac{49}{2}^+$	6530.0	0.91(9)	38(5)	
798.7	$\frac{57}{2}^+ \rightarrow \frac{53}{2}^+$	7328.7	0.96(10)	27(4)	
854.5	$\frac{61}{2}^+ \rightarrow \frac{57}{2}^+$	8183.3	1.10(17)[e]	13(3)	
941.2	$\frac{61}{2}^+ \rightarrow \frac{57}{2}^+$		1.05(21)	$\leqslant$3	9
926.0	$\frac{65}{2}^+ \rightarrow \frac{61}{2}^+$	9109.3	0.98(15)	9(2)	
880.1	$\frac{65}{2}^+ \rightarrow \frac{61}{2}^+$			4(2)	5
959.0	$\frac{69}{2}^+ \rightarrow \frac{65}{2}^+$	10068.3	0.96(19)	7(2)	
1016.4	$\frac{73}{2}^+ \rightarrow \frac{69}{2}^+$	11084.7	1.17(23)	6(2)	
1075.9	$\frac{77}{2}^+ \rightarrow \frac{73}{2}^+$	12160.6	1.13(23)	5(1)	
1135.1	$(\frac{81}{2}^+) \rightarrow \frac{77}{2}^+$	13295.6		4(1)	
1192.4	$(\frac{85}{2}^+) \rightarrow (\frac{81}{2}^+)$	14488.0		$\leqslant$3	
1247.2	$(\frac{89}{2}^+) \rightarrow (\frac{85}{2}^+)$	15735.0		$\leqslant$3	
(1313.1)	$(\frac{93}{2}^+) \rightarrow (\frac{89}{2}^+)$	17047.7		$\leqslant$3	
	Band 12				
719.8	$\frac{35}{2}^+ \rightarrow \frac{33}{2}^+$	3974.4	0.66(10)		11
547.0	$\frac{39}{2}^+ \rightarrow \frac{35}{2}^+$	4521.4	0.92(18)	18(3)	
706.1	$\frac{39}{2}^+ \rightarrow \frac{37}{2}^+$		0.66(13)	8(2)	11
604.3	$\frac{43}{2}^+ \rightarrow \frac{39}{2}^+$	5126.3		14(3)	
704.2	$\frac{43}{2}^+ \rightarrow \frac{41}{2}^+$			5(2)	11
658.1	$\frac{47}{2}^+ \rightarrow \frac{43}{2}^+$	5784.4	0.87(13)	10(2)	
707.7	$\frac{47}{2}^+ \rightarrow \frac{45}{2}^+$			4(1)	11
710.8	$\frac{51}{2}^+ \rightarrow \frac{47}{2}^+$	6495.2	1.00(20)	7(1)	

TABLE IV. (*Continued.*)

E_γ[a]	$I_i^\pi \rightarrow I_f^\pi$[b]	E_i	DCO[c]	I_γ[d]	N
717.0	$\frac{51}{2}^+ \rightarrow \frac{49}{2}^+$			4(1)	11
765.0	$\frac{55}{2}^+ \rightarrow \frac{51}{2}^+$	7260.3	1.06(21)	6(2)	
730.3	$\frac{55}{2}^+ \rightarrow \frac{53}{2}^+$			$\leqslant$3	11
816.0	$\frac{59}{2}^+ \rightarrow \frac{55}{2}^+$	8076.2	1.03(20)	6(2)	
870.1	$\frac{63}{2}^+ \rightarrow \frac{59}{2}^+$	8946.3	0.94(19)	5(1)	
923.0	$\frac{67}{2}^+ \rightarrow \frac{63}{2}^+$	9869.2	1.05(21)	5(1)	
977.4	$(\frac{71}{2}^+) \rightarrow \frac{67}{2}^+$	10846.2		3	
1032.3	$(\frac{75}{2}^+) \rightarrow (\frac{71}{2}^+)$	11878.3		$\leqslant$3	
1084.0	$(\frac{79}{2}^+) \rightarrow (\frac{75}{2}^+)$	12962.2		$\leqslant$3	
1149.2	$(\frac{83}{2}^+) \rightarrow (\frac{79}{2}^+)$	14111.3		$\leqslant$3	
1200.1	$(\frac{87}{2}^+) \rightarrow (\frac{81}{2}^+)$	15311.3		$\leqslant$3	
	Band 13				
87.7	$\frac{1}{2}^- \rightarrow \frac{3}{2}^+$	136.5			8
102.6	$\frac{1}{2}^- \rightarrow \frac{1}{2}^+$		0.92(4)	112(22)	8
225.0	$\frac{3}{2}^- \rightarrow \frac{1}{2}^+$	258.8		17(3)	8
107.3	$\frac{5}{2}^- \rightarrow \frac{3}{2}^+$	156.1	0.84(3)	263(53)	8
176.7	$\frac{7}{2}^- \rightarrow \frac{3}{2}^-$	435.5	1.07(5)	10(2)	
279.4	$\frac{7}{2}^- \rightarrow \frac{5}{2}^-$			110(22)	
167.7	$\frac{7}{2}^- \rightarrow \frac{9}{2}^-$			25(7)	
111.7	$\frac{9}{2}^- \rightarrow \frac{5}{2}^-$	267.8		291(58)	
257.4	$\frac{11}{2}^- \rightarrow \frac{7}{2}^-$	693.0	1.04(5)	64(13)	
425.2	$\frac{11}{2}^- \rightarrow \frac{9}{2}^-$			88(18)	
213.0	$\frac{11}{2}^- \rightarrow \frac{13}{2}^-$			7(2)	
212.3	$\frac{13}{2}^- \rightarrow \frac{9}{2}^-$	480.1	1.10(4)	663(61)	
341.6	$\frac{15}{2}^- \rightarrow \frac{11}{2}^-$	1034.6	1.08(11)	68(6)	
554.6	$\frac{15}{2}^- \rightarrow \frac{13}{2}^-$		0.58(9)	24(2)	
314.5	$\frac{17}{2}^- \rightarrow \frac{13}{2}^-$	794.7	1.02(4)	875(81)	
424.6	$\frac{19}{2}^- \rightarrow \frac{15}{2}^-$	1459.2	1.05(11)	69(8)	
664.5	$\frac{19}{2}^- \rightarrow \frac{17}{2}^-$		0.55(8)	23(1)	
410.8	$\frac{21}{2}^- \rightarrow \frac{17}{2}^-$	1205.5	0.93(4)	1000(14)	
501.1	$\frac{23}{2}^- \rightarrow \frac{19}{2}^-$	1960.3	1.03(4)	80(16)	
754.1	$\frac{23}{2}^- \rightarrow \frac{21}{2}^-$			27(1)	
498.2	$\frac{25}{2}^- \rightarrow \frac{21}{2}^-$	1703.5	1.03(4)	936(14)	
566.8	$\frac{27}{2}^- \rightarrow \frac{23}{2}^-$	2527.1	1.04(4)	86(17)	
823.4	$\frac{27}{2}^- \rightarrow \frac{25}{2}^-$			25(1)	
574.7	$\frac{29}{2}^- \rightarrow \frac{25}{2}^-$	2278.3	1.03(4)	716(13)	
612.0	$\frac{31}{2}^- \rightarrow \frac{27}{2}^-$	3139.0	1.05(11)	54(5)	
860.4	$\frac{31}{2}^- \rightarrow \frac{29}{2}^-$			15(1)	
640.9	$\frac{33}{2}^- \rightarrow \frac{29}{2}^-$	2918.8	1.05(4)	508(12)	
591.3	$\frac{35}{2}^- \rightarrow \frac{31}{2}^-$	3730.3	1.07(11)	57(6)	
695.8	$\frac{37}{2}^- \rightarrow \frac{33}{2}^-$	3613.4	1.01(4)	324(69)	
536.4	$\frac{39}{2}^- \rightarrow \frac{35}{2}^-$	4266.7	0.93(14)	47(11)	

TABLE IV. (*Continued.*)

E_γ[a]	$I_i^\pi \rightarrow I_f^\pi$[b]	E_i	DCO[c]	I_γ[d]	N
760.0	$\frac{41}{2}^- \rightarrow \frac{37}{2}^-$	4373.4	0.95(4)	130(14)	
603.3	$\frac{41}{2}^- \rightarrow \frac{37}{2}^-$		0.93(19)	15(3)	14
572.6	$\frac{43}{2}^- \rightarrow \frac{39}{2}^-$	4838.7	1.04(10)	51(5)	
594.0	$\frac{43}{2}^- \rightarrow \frac{39}{2}^-$		0.81(15)	21(2)	3
613.7	$\frac{43}{2}^- \rightarrow \frac{39}{2}^-$			15(2)	16
768.8	$\frac{45}{2}^- \rightarrow \frac{41}{2}^-$	5142.2	1.04(21)[e]	8(2)	
836.2	$\frac{45}{2}^- \rightarrow \frac{41}{2}^-$		1.03(16)	24(2)	14
652.6	$\frac{47}{2}^- \rightarrow \frac{43}{2}^-$	5490.4	1.02(10)	69(7)	
765.1	$\frac{49}{2}^- \rightarrow \frac{45}{2}^-$	5907.3	1.04(8)[e]	8(2)	
714.8	$\frac{51}{2}^- \rightarrow \frac{47}{2}^-$	6205.2	1.05(11)	69(7)	
726.6	$\frac{53}{2}^- \rightarrow \frac{49}{2}^-$	6633.9	1.06(21)	8(2)	
763.2	$\frac{55}{2}^- \rightarrow \frac{51}{2}^-$	6968.5	1.08(11)	56(7)	
776.6	$\frac{57}{2}^- \rightarrow \frac{53}{2}^-$	7410.5	1.02(20)	4(2)	
810.3	$\frac{59}{2}^- \rightarrow \frac{55}{2}^-$	7778.6	1.09(16)	30(3)	
845.1	$\frac{61}{2}^- \rightarrow \frac{57}{2}^-$	8255.6	1.02(20)	$\leqslant$3	
865.0	$\frac{63}{2}^- \rightarrow \frac{59}{2}^-$	8642.7	1.05(21)	19(2)	
917.5	$(\frac{65}{2}^-) \rightarrow \frac{61}{2}^-$	9173.1		$\leqslant$3	
923.7	$\frac{67}{2}^- \rightarrow \frac{63}{2}^-$	9565.4	1.10(22)	12(2)	
971.5	$(\frac{69}{2}^-) \rightarrow (\frac{65}{2}^-)$	10144.6		$\leqslant$3	
984.9	$(\frac{71}{2}^-) \rightarrow \frac{67}{2}^-$	10549.8		$\leqslant$3	
1007.0	$(\frac{73}{2}^-) \rightarrow (\frac{69}{2}^-)$	11152.0		$\leqslant$3	
1048.1	$(\frac{75}{2}^-) \rightarrow (\frac{71}{2}^-)$	11597.3		$\leqslant$3	
(1057.9)	$(\frac{77}{2}^-) \rightarrow (\frac{73}{2}^-)$	12210.0		$\leqslant$3	
1096.1	$(\frac{79}{2}^-) \rightarrow (\frac{75}{2}^-)$	12693.7		$\leqslant$3	
1115.9	$(\frac{83}{2}^-) \rightarrow (\frac{79}{2}^-)$	13809.6		$\leqslant$3	
	Band 14				
1370.0	$\frac{21}{2}^- \rightarrow \frac{17}{2}^-$	2165.2		6(1)	13
318.4	$\frac{25}{2}^- \rightarrow \frac{21}{2}^-$	2483.7	1.10(20)	16(2)	
1278.1	$\frac{25}{2}^- \rightarrow \frac{21}{2}^-$		1.11(22)	15(2)	13
410.8	$\frac{29}{2}^- \rightarrow \frac{25}{2}^-$	2894.5	0.93(5)	$\sim$80	
1191.1	$\frac{29}{2}^- \rightarrow \frac{25}{2}^-$		1.03(21)	15(2)	13
399.4	$\frac{33}{2}^- \rightarrow \frac{29}{2}^-$	3294.0	0.97(10)	76(16)	
1016.0	$\frac{33}{2}^- \rightarrow \frac{29}{2}^-$			12(3)	13
476.0	$\frac{37}{2}^- \rightarrow \frac{33}{2}^-$	3770.1	1.01(4)	64(13)	
851.3	$\frac{37}{2}^- \rightarrow \frac{33}{2}^-$		0.95(19)	19(2)	13
536.0	$\frac{41}{2}^- \rightarrow \frac{37}{2}^-$	4306.0		65(9)	
692.6	$\frac{41}{2}^- \rightarrow \frac{37}{2}^-$		1.04(4)	115(20)	13
635.9	$\frac{45}{2}^- \rightarrow \frac{41}{2}^-$	4941.9	1.05(4)	109(10)	
568.4	$\frac{45}{2}^- \rightarrow \frac{41}{2}^-$			14(3)	13
696.2	$\frac{49}{2}^- \rightarrow \frac{45}{2}^-$	5637.9	1.00(4)	100(20)	
759.6	$\frac{53}{2}^- \rightarrow \frac{49}{2}^-$	6397.5	0.97(10)	77(19)	
817.6	$\frac{57}{2}^- \rightarrow \frac{53}{2}^-$	7215.0	1.00(10)	68(17)	

TABLE IV. (*Continued.*)

E_γ [a]	$I_i^\pi \rightarrow I_f^\pi$ [b]	E_i	DCO [c]	I_γ [d]	N
872.6	$\frac{61}{2}^- \rightarrow \frac{57}{2}^-$	8087.6	0.96(9)	54(13)	
926.6	$\frac{65}{2}^- \rightarrow \frac{61}{2}^-$	9014.2	0.98(15)	38(10)	
980.0	$\frac{69}{2}^- \rightarrow \frac{65}{2}^-$	9992.4	1.02(15)	24(6)	
976.9	$\frac{69}{2}^- \rightarrow \frac{65}{2}^-$			$\leqslant 3$	2
1033.9	$\frac{73}{2}^- \rightarrow \frac{69}{2}^-$	11026.2	0.95(19)	8(3)	
1100.1	$(\frac{77}{2}^-) \rightarrow \frac{73}{2}^-$	12126.3		$\leqslant 3$	
1090.1	$(\frac{77}{2}^-) \rightarrow \frac{73}{2}^-$			$\leqslant 3$	2
1150.9	$(\frac{81}{2}^-) \rightarrow (\frac{77}{2}^-)$	13277.1		$\leqslant 3$	
(1139.1)	$(\frac{81}{2}^-) \rightarrow \frac{77}{2}^-$			$\leqslant 3$	2
1188.2	$(\frac{85}{2}^-) \rightarrow (\frac{81}{2}^-)$	14465.2		$\leqslant 3$	
	Band 15				
331.9	$\frac{9}{2}^- \rightarrow \frac{7}{2}^+$	331.9		404(60)	1
191.7	$\frac{9}{2}^- \rightarrow \frac{9}{2}^+$			321(64)	1
101.5	$\frac{11}{2}^- \rightarrow \frac{9}{2}^-$	433.6		101(20)	
293.6	$\frac{11}{2}^- \rightarrow \frac{9}{2}^+$			330(66)	1
245.1	$\frac{13}{2}^- \rightarrow \frac{9}{2}^-$	577.0		144(24)	
143.4	$\frac{13}{2}^- \rightarrow \frac{11}{2}^-$			448(28)	
310.4	$\frac{15}{2}^- \rightarrow \frac{11}{2}^-$	744.3		328(24)	
167.3	$\frac{15}{2}^- \rightarrow \frac{13}{2}^-$			629(55)	
370.8	$\frac{17}{2}^- \rightarrow \frac{13}{2}^-$	947.9		336(29)	
203.6	$\frac{17}{2}^- \rightarrow \frac{15}{2}^-$			494(29)	
415.3	$\frac{19}{2}^- \rightarrow \frac{15}{2}^-$	1159.6		481(29)	
211.7	$\frac{19}{2}^- \rightarrow \frac{17}{2}^-$			463(34)	
463.8	$\frac{21}{2}^- \rightarrow \frac{17}{2}^-$	1411.7		426(26)	
252.1	$\frac{21}{2}^- \rightarrow \frac{19}{2}^-$			396(32)	
496.4	$\frac{23}{2}^- \rightarrow \frac{19}{2}^-$	1656.0		482(29)	
244.4	$\frac{23}{2}^- \rightarrow \frac{21}{2}^-$			320(30)	
535.9	$\frac{25}{2}^- \rightarrow \frac{21}{2}^-$	1947.6		425(27)	
291.6	$\frac{25}{2}^- \rightarrow \frac{23}{2}^-$			252(16)	
558.9	$\frac{27}{2}^- \rightarrow \frac{23}{2}^-$	2214.9		467(29)	
267.6	$\frac{27}{2}^- \rightarrow \frac{25}{2}^-$			142(25)	
584.4	$\frac{29}{2}^- \rightarrow \frac{25}{2}^-$	2532.1		301(38)	
316.4	$\frac{29}{2}^- \rightarrow \frac{27}{2}^-$			200(29)	
585.8	$\frac{31}{2}^- \rightarrow \frac{27}{2}^-$	2800.7		478(51)	
268.4	$\frac{31}{2}^- \rightarrow \frac{29}{2}^-$			348(60)	
538.2	$\frac{33}{2}^- \rightarrow \frac{29}{2}^-$	3070.3		257(18)	
269.6	$\frac{33}{2}^- \rightarrow \frac{31}{2}^-$			378(60)	
488.3	$\frac{35}{2}^- \rightarrow \frac{31}{2}^-$	3289.0		221(14)	
218.8	$\frac{35}{2}^- \rightarrow \frac{33}{2}^-$			244(15)	
453.1	$\frac{37}{2}^- \rightarrow \frac{33}{2}^-$	3523.4		174(11)	
234.4	$\frac{37}{2}^- \rightarrow \frac{35}{2}^-$			249(15)	

TABLE IV. (*Continued.*)

E_γ [a]	$I_i^\pi \rightarrow I_f^\pi$ [b]	E_i	DCO [c]	I_γ [d]	N
485.3	$\frac{39}{2}^- \rightarrow \frac{35}{2}^-$	3774.3		161(12)	
251.0	$\frac{39}{2}^- \rightarrow \frac{37}{2}^-$			172(17)	
522.4	$\frac{41}{2}^- \rightarrow \frac{37}{2}^-$	4046.0		209(14)	
271.7	$\frac{41}{2}^- \rightarrow \frac{39}{2}^-$			209(14)	
565.2	$\frac{43}{2}^- \rightarrow \frac{39}{2}^-$	4339.7		166(12)	
293.9	$\frac{43}{2}^- \rightarrow \frac{41}{2}^-$			145(16)	
610.2	$\frac{45}{2}^- \rightarrow \frac{41}{2}^-$	4656.2		202(14)	
316.9	$\frac{45}{2}^- \rightarrow \frac{43}{2}^-$			134(21)	
646.7	$\frac{47}{2}^- \rightarrow \frac{43}{2}^-$	4986.2		181(15)	
330.0	$\frac{47}{2}^- \rightarrow \frac{45}{2}^-$			138(12)	
693.0	$\frac{49}{2}^- \rightarrow \frac{45}{2}^-$	5349.1		174(24)	
363.0	$\frac{49}{2}^- \rightarrow \frac{47}{2}^-$			90(18)	
719.6	$\frac{51}{2}^- \rightarrow \frac{47}{2}^-$	5705.5		187(25)	
356.4	$\frac{51}{2}^- \rightarrow \frac{49}{2}^-$			87(7)	
767.9	$\frac{53}{2}^- \rightarrow \frac{49}{2}^-$	6116.8		117(10)	
411.8	$\frac{53}{2}^- \rightarrow \frac{51}{2}^-$			38(5)	
784.8	$\frac{55}{2}^- \rightarrow \frac{51}{2}^-$	6490.3		102(9)	
373.8	$\frac{55}{2}^- \rightarrow \frac{53}{2}^-$			33(4)	
836.2	$\frac{57}{2}^- \rightarrow \frac{53}{2}^-$	6953.0		101(10)	
462.7	$\frac{57}{2}^- \rightarrow \frac{55}{2}^-$			87(10)	
844.4	$\frac{59}{2}^- \rightarrow \frac{55}{2}^-$	7334.7		74(8)	
381.7	$\frac{59}{2}^- \rightarrow \frac{57}{2}^-$			22(2)	
902.1	$\frac{61}{2}^- \rightarrow \frac{57}{2}^-$	7855.1	1.08(5)	89(9)	
520.4	$\frac{61}{2}^- \rightarrow \frac{59}{2}^-$		0.95(19)	10(3)	
901.4	$\frac{63}{2}^- \rightarrow \frac{59}{2}^-$	8236.1	0.94(9)	60(7)	
381.0	$\frac{63}{2}^- \rightarrow \frac{61}{2}^-$		0.61(12)	16(2)	
968.9	$\frac{65}{2}^- \rightarrow \frac{61}{2}^-$	8824.0	1.00(15)	48(5)	
588.0	$\frac{65}{2}^- \rightarrow \frac{63}{2}^-$			13(2)	
956.4	$\frac{67}{2}^- \rightarrow \frac{63}{2}^-$	9192.5	1.01(15)	48(5)	
368.4	$\frac{67}{2}^- \rightarrow \frac{65}{2}^-$		0.75(6)	13(2)	
1034.1	$\frac{69}{2}^- \rightarrow \frac{65}{2}^-$	9858.4	1.04(16)	30(4)	
1010.3	$\frac{71}{2}^- \rightarrow \frac{67}{2}^-$	10202.5	0.99(15)	34(4)	
1089.0	$\frac{73}{2}^- \rightarrow \frac{69}{2}^-$	10947.4	1.00(15)	20(3)	
1062.4	$\frac{75}{2}^- \rightarrow \frac{71}{2}^-$	11264.6	0.97(19)	16(2)	
1102.2	$\frac{77}{2}^- \rightarrow \frac{73}{2}^-$	12050.0	0.98(20)	11(3)	
1111.9	$\frac{79}{2}^- \rightarrow \frac{75}{2}^-$	12377.0	1.03(21)	11(4)	
1108.3	$\frac{81}{2}^- \rightarrow \frac{77}{2}^-$	13158.4	1.01(22)	8(3)	
1160.1	$\frac{83}{2}^- \rightarrow \frac{79}{2}^-$	13536.6	0.97(19)	5(2)	
1141.9	$(\frac{85}{2}^-) \rightarrow \frac{81}{2}^-$	14300.0		$\leqslant 3$	
1200.2	$\frac{87}{2}^- \rightarrow \frac{83}{2}^-$	14736.6	0.91(18)	$\leqslant 3$	
1173.1	$(\frac{89}{2}^-) \rightarrow (\frac{85}{2}^-)$	15472.9		$\leqslant 3$	
1231.0	$(\frac{91}{2}^-) \rightarrow \frac{87}{2}^-$	15967.9		$\leqslant 3$	

TABLE IV. (*Continued.*)

E_γ[a]	$I_i^\pi \rightarrow I_f^\pi$[b]	E_i	DCO[c]	I_γ[d]	N
1208.4	$(\frac{93}{2}^-) \rightarrow (\frac{89}{2}^-)$	16681.2		$\leqslant 3$	
1261.3	$(\frac{95}{2}^-) \rightarrow (\frac{91}{2}^-)$	17229.3		$\leqslant 3$	
(1262.1)	$(\frac{97}{2}^-) \rightarrow (\frac{93}{2}^-)$	17943.3		$\leqslant 3$	
	Band 16				
677.0	$\frac{35}{2}^- \rightarrow \frac{31}{2}^-$	3477.7		~25(5)[e]	15
747.3	$\frac{39}{2}^- \rightarrow \frac{35}{2}^-$	4225.0		~23(5)[e]	
329.2		4554.2		20(4)	
676.2		5230.4		~15(3)[e]	
682.5		5912.9		14(3)	
746.4		6659.3		~13(3)[e]	
752.0				$\leqslant 3$	13
801.9		7461.2		6(2)	
859.2		8320.4		$\leqslant 3$	
912.0		9232.4		$\leqslant 3$	
952.6		10185.0		$\leqslant 3$	
1009.1		11194.1		$\leqslant 3$	
	Band 17				
768.0			0.84(31)	$\leqslant 3$	
814.8			0.96(18)	$\leqslant 3$	
876.2			0.95(19)	$\leqslant 3$	
930.0			0.99(20)	$\leqslant 3$	
984.7			0.98(20)	$\leqslant 3$	
1039.5			0.98(20)	$\leqslant 3$	

TABLE IV. (*Continued.*)

E_γ[a]	$I_i^\pi \rightarrow I_f^\pi$[b]	E_i	DCO[c]	I_γ[d]	N
1096.2			0.94(19)	$\leqslant 3$	
1153.1			0.97(18)	$\leqslant 3$	
1210.4			1.00(20)	$\leqslant 3$	
1264.0			0.97(19)	$\leqslant 3$	
1309.3			1.11(29)	$\leqslant 3$	
1356.1				$\leqslant 3$	
	Band 18				
807.0				$\leqslant 3$	
863.1				$\leqslant 3$	
918.3				$\leqslant 3$	
974.5				$\leqslant 3$	
1030.1				$\leqslant 3$	
1089.3				$\leqslant 3$	
1148.2				$\leqslant 3$	
1210.0				$\leqslant 3$	
1270.2				$\leqslant 3$	

[a]Uncertainties in γ-ray energies are 0.2 keV for most transitions, except for relatively weak transitions (<10 units) where 0.5-keV uncertainties are appropriate.

[b]Less certain I^π assignments are given in parentheses.

[c]DCO ratio from gated spectra; see Sec. II for details.

[d]Relative intensities are normalized to the 410.8-keV ($\frac{21}{2}^- \rightarrow \frac{17}{2}^-$) transition ($\equiv 1000$) in Band 13.

[e]Unresolved multiplet.

[1] A. Bohr and B. R. Mottleson, *Nuclear Structure*, Vol. II, (Benjamin, New York, 1975).

[2] S. W. Ødegård, G. B. Hagemann, D. R. Jensen, M. Bergström, B. Herskind, G. Sletten, S. Törmänen, J. N. Wilson, P. O. Tjöm, I. Hamamoto, K. Spohr, H. Hübel, A. Görgen, G. Schönwasser, A. Bracco, S. Leoni, A. Maj, C. M. Petrache, P. Bednarczyk, and D. Curien, Phys. Rev. Lett. **86**, 5866 (2001).

[3] D. R. Jensen, G. B. Hagemann, I. Hamamoto, S. W. Ødegärd, B. Herskind, G. Sletten, J. N. Wilson, K. Spohr, H. Hübel, P. Bringel, A. Neußer, G. Schönwaßer, A. K. Singh, W. C. Ma, H. Amro, A. Bracco, S. Leoni, G. Benzoni, A. Maj, C. M. Petrache, G. Lo Bianco, P. Bednarczyk, and D. Curien, Phys. Rev. Lett. **89**, 142503 (2002).

[4] G. Schönwaßer *et al.*, Phys. Lett. B **552**, 9 (2003).

[5] H. Amro *et al.*, Phys. Lett. B **553**, 197 (2003).

[6] P. Bringel *et al.*, Eur. Phys. J. A **24**, 167 (2005).

[7] D. J. Hartley, R. V. F. Janssens, L. L. Riedinger, M. A. Riley, A. Aguilar, M. P. Carpenter, C. J. Chiara, P. Chowdhury, I. G. Darby, U. Garg, Q. A. Ijaz, F. G. Kondev, S. Lakshmi, T. Lauritsen, A. Ludington, W. C. Ma, E. A. McCutchan, S. Mukhopadhyay, R. Pifer, E. P. Seyfried, I. Stefanescu, S. K. Tandel, U. Tandel, J. R. Vanhoy, X. Wang, S. Zhu, I. Hamamoto, and S. Frauendorf, Phys. Rev. C **80**, 041304(R) (2009).

[8] D. R. Jensen *et al.*, Nucl. Phys **A703**, 3 (2002).

[9] D. R. Jensen *et al.*, Eur. Phys. J. A **19**, 173 (2004).

[10] P. Bringel, C. Engelhardt, H. Hübel, A. Neußer-Neffgen, S. W. Ødegärd, G. B. Hagemann, C. R. Hansen, B. Herskind, G. Sletten, M. P. Carpenter, R. V. F. Janssens, T. L. Khoo, T. Lauritsen, D. Seweryniak, W. C. Ma, D. G. Roux, and P. Chowdhury, Phys. Rev. C **75**, 044306 (2007).

[11] J. C. Marsh, W. C. Ma, G. B. Hagemann, R. V. F. Janssens, R. Bengtsson, H. Ryde, M. P. Carpenter, G. Gürdal, D. J. Hartley, C. R. Hoffman, Q. A. Ijaz, F. G. Kondev, T. Lauritsen, S. Mukhopadhyay, L. L. Riedinger, R. B. Yadav, and S. Zhu, Phys. Rev. C **88**, 041306(R) (2013).

[12] H. Amro *et al.*, Phys. Lett. B **506**, 39 (2001).

[13] R. B. Yadav, W. C. Ma, G. B. Hagemann, R. Bengtsson, H. Ryde, H. Amro, A. Bracco, M. P. Carpenter, J. Domscheit, S. Frattini, D. J. Hartley, B. Herskind, H. Hubel, R. V. F. Janssens, T. L. Khoo, F. G. Kondev, T. Lauritsen, C. J. Lister, B. Million, S. Odegard, L. L. Riedinger, K. A. Schmidt, S. Siem, G. Sletten, P. G. Varmette, J. N. Wilson, and Y. C. Zhang, Phys. Rev. C **78**, 044316 (2008).

[14] T. Bengtsson, Nucl. Phys. A **496**, 56 (1989).

[15] T. Bengtsson, Nucl. Phys. A **512**, 124 (1990).

[16] R. Bengtsson, www.matfys.lth.se/staff/Ragnar.Bengtsson/TSD.html

[17] H. Schnack-Peterson *et al.*, Nucl. Phys. A **594**, 175 (1995).
[18] R. Bengtsson and H. Ryde, Eur. Phys. J. A **22**, 355 (2004).
[19] I. Hamamoto, Phys. Rev. C **65**, 044305 (2002).
[20] I. Hamamoto and G. B. Hagemann, Phys. Rev. C **67**, 014319 (2003).
[21] N. S. Pattabiraman *et al.*, Phys. Lett. B **647**, 243 (2007).
[22] X. Wang, R. V. F. Janssens, E. F. Moore, U. Garg, Y. Gu, S. Frauendorf, M. P. Carpenter, S. S. Ghugre, N. J. Hammond, T. Lauritsen, T. Li, G. Mukherjee, N. S. Pattabiraman, D. Seweryniak, and S. Zhu, Phys. Rev. C **75**, 064315 (2007).
[23] H. Amro, G. B. Hagemann, W. C. Ma, R. M. Diamond, J. Domscheit, P. Fallon, B. Herskind, H. Hübel, D. R. Jensen, Y. Li, A. O. Macchiavelli, D. Roux, G. Sletten, J. Thompson, I. Wiedenhöver, J. N. Wilson, and J. A. Winger, Phys. Rev. C **71**, 011302 (2005).
[24] D. C. Radford, Nucl. Instrum. Methods A **361**, 297 (1995).
[25] K. S. Krane, R. M. Steffen, and R. M. Wheeler, Nucl. Data Tables **11**, 351 (1973).
[26] R. B. Yadav, W. C. Ma, G. B. Hagemann, H. Amro, A. Bracco, M. P. Carpenter, J. Domscheit, S. Frattini, D. J. Hartley, B. Herskind, H. Hübel, R. V. F. Janssens, T. L. Khoo, F. G. Kondev, T. Lauritsen, C. J. Lister, B. Million, S. Ødegård, L. L. Riedinger, K. A. Schmidt, S. Siem, G. Sletten, P. G. Varmette, J. N. Wilson, and Y. C. Zhang, Phys. Rev. C **80**, 064306 (2009).
[27] D. Barnéoud and C. Foin, Nucl. Phys. A **287**, 77 (1977).
[28] C. H. Yu *et al.*, Nucl. Phys. A **511**, 157 (1990).
[29] C. Ekström, S. Ingelman, B. Wannberg, and I. L. Lamm, Phys. Lett. B **39**, 199 (1972).
[30] W. C. Ma *et al.* (unpublished).
[31] G. Schönwaßer *et al.*, Nucl. Phys. A **735**, 393 (2004).
[32] D. J. Hartley, W. H. Mohr, J. R. Vanhoy, M. A. Riley, A. Aguilar, C. Teal, R. V. F. Janssens, M. P. Carpenter, A. A. Hecht, T. Lauritsen, E. F. Moore, S. Zhu, F. G. Kondev, M. K. Djongolov, M. Danchev, L. L. Riedinger, G. B. Hagemann, G. Sletten, P. Chowdhury, S. K. Tandel, W. C. Ma, and S. W. Ødegård, Phys. Rev. C **74**, 054314 (2006).
[33] D. R. Jensen *et al.*, Eur. Phys. J. A **8**, 165 (2000).
[34] H. J. Jensen *et al.*, Nucl. Phys. A **695**, 3 (2001).
[35] D. J. Hartley, W. H. Mohr, J. R. Vanhoy, M. A. Riley, A. Aguilar, C. Teal, R. V. F. Janssens, M. P. Carpenter, A. Hecht, T. Lauritsen, E. F. Moore, S. Zhu, F. G. Kondev, M. K. Djongolov, M. Danchev, L. L. Riedinger, G. B. Hagemann, G. Sletten, P. Chowdhury, S. K. Tandel, W. C. Ma, and S. W. Ødegård, Phys. Rev. C **72**, 064325 (2005).
[36] E. M. Beck *et al.*, Z. Phys. A **327**, 397 (1987).
[37] G. Gürdal *et al.*, J. Phys. G **31**, S1873 (2005).
[38] S. Ogaza *et al.*, Nucl. Phys. A **559**, 100 (1993).
[39] R. A. Bark *et al.*, Nucl. Phys. A **644**, 29 (1998).
[40] H. Carlsson *et al.*, Nucl. Phys. A **592**, 89 (1995).
[41] G. B. Hagemann, I. Hamamoto, and W. Satula, Phys. Rev. C **47**, 2008 (1993).
[42] L. D. Landau, Phys. Z. Sov. **2**, 46 (1932); C. Zener, Proc. R. Soc. London A **137**, 696 (1932).
[43] D. J. Hartley, R. V. F. Janssens, L. L. Riedinger, M. A. Riley, X. Wang, A. Aguilar, M. P. Carpenter, C. J. Chiara, P. Chowdhury, I. G. Darby, U. Garg, Q. A. Ijaz, F. G. Kondev, S. Lakshmi, T. Lauritsen, A. Ludington, W. C. Ma, E. A. McCutchan, S. Mukhopadhyay, R. Pifer, E. P. Seyfried, U. Shirwadkar, I. Stefanescu, S. K. Tandel, J. R. Vanhoy, S. Zhu, and S. Frauendorf, Phys. Rev. C **83**, 064307 (2011).
[44] D. G. Roux, M. S. Fetea, E. Gueorguieva, B. R. S. Babu, R. T. Newman, J. J. Lawrie, R. Fearick, D. G. Aschman, R. Beetge, M. Benatar, G. K. Mabala, S. M. Mullins, S. H. T. Murray, S. Naguleswaran, C. Rigollet, J. F. Sharpey-Schafer, F. D. Smit, and W. J. Whittaker, Phys. Rev. C **63**, 024303 (2001).
[45] A. Neußer-Neffgen *et al.*, Phys. Rev. C **73**, 034309 (2006).
[46] K. A. Schmidt *et al.*, Eur. Phys. J. A **12**, 15 (2001).